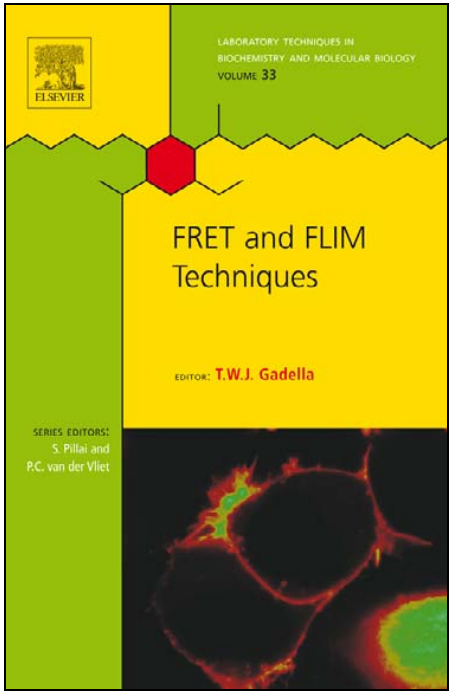

From: Kees Jalink and Jacco van Rheenen, FilterFRET: Quantitative imaging of sensitized emission.
In T. W. J. Gadella, editor, Laboratory Techniques in Biochemistry and Molecular Biology, Vol 33, Burlington: Academic Press, 2009, pp.289-349.
ISBN: 978-0-08-054958-3

Laboratory Techniques in Biochemistry and Molecular Biology, Volume 33
FRET and FLIM Techniques
T. W. J. Gadella (Editor)

CHAPTER 7

FilterFRET: Quantitative imaging of sensitized emission

Kees Jalink[1] and Jacco van Rheenen[2]

[1]*Department of Cell Biology, The Netherlands Cancer Institute, Plesmanlaan 121, 1066 CX Amsterdam, The Netherlands*
[2]*Hubrecht Institute-KNAW and University Medical Center Utrecht, Uppsalalaan 8, 3584CT, Utrecht, The Netherlands*

Previous chapters in this volume were dedicated to advanced imaging techniques such as fluorescence lifetime imaging (FLIM) that require complicated, dedicated, and expensive equipment. Fluorescence resonance energy transfer (FRET) can also be assessed from simple fluorescence images taken with conventional wide-field or confocal microscopes readily available in most research institutes. To this goal, cells expressing donor- and acceptor-tagged proteins ("FRET cells") are imaged, along with control cells expressing either donor- or acceptor alone, under different spectral recording conditions (i.e., with different filter sets). Quantitative FRET images are then calculated by mathematically correcting for filter leak-through terms. Algorithms for "filterFRET" with wide-field microscopes have been reported by several groups but for confocal imaging, separate formalisms had to be developed.

In this chapter, we intend to give the reader an understanding of the possibilities and pitfalls of filterFRET. Following a brief historical overview describing early nonquantitative incarnations of FRET imaging, the theory that allows quantitative wide-field and

DOI: 10.1016/S0075-7535(08)00007-7

confocal FRET imaging will be treated. Special emphasis will be on calibration of the FRET setup and images. Next, major sources of error and noise that have hampered, until recently, application of these algorithms in a very quantitative way will be discussed. Finally, image enhancement strategies, their possible bias on the results and some useful presentation aids will be treated. Taken together, with proper attention for image recording conditions and enhancement strategies, imaging of sensitized emission is a quantitative, fast, photon-efficient, and easy way to determine FRET.

7.1. Introduction

7.1.1. Definition

The term filterFRET here refers to intensity-based methods for calculating fluorescence resonance energy transfer (FRET) from sets of images of the preparation collected at different excitation and/or emission wavelength. The term is not intended to imply that interference filters are actually present in the setup; very similar considerations apply when donor- and acceptor fluorophores are spectrally resolved by other means, such as monochromators or spectral detectors.

7.1.2. Sensitized emission

In previous chapters it was shown that FRET can be reliably detected by donor fluorescence lifetime imaging. Here, we will focus on what is perhaps the most intuitive and straightforward way to record FRET: imaging of sensitized emission (s.e., that is, the amount of acceptor emission that results from energy transferred by the donor through resonance) by filterFRET. While simple in principle, determinations of s.e. are complicated by overlap of excitation and emission spectra of the donors and acceptors, and by several imperfections of the recording optics, light sources and detectors.

7.1.3. The sensitized emission problem

To explain what problems complicate filterFRET, consider the model neuronal cell in Fig. 7.1A. It contains two independently expressed fluorophores: donor molecules at the membrane and in the nucleus, and acceptor molecules at the membrane and around the nucleus. Thus, FRET is only possible at the membrane and sensitized emission should be restricted to the membrane. However, if we collect an s.e. image (**S**) by exciting donors while collecting the fluorescence of acceptors (Fig. 7.1A) the intensity distribution differs from the predicted FRET distribution (compare the s.e. panel, bottom right, to the FRET panel). In particular, **S** also shows some signal from donors in the nucleus and from acceptors in the region around the nucleus. This is due to overlap of the excitation and emission spectra (Fig. 7.1B), which is particularly apparent when genetically encoded fluorescent proteins (FPs) are used as labels. First, overlap of the donor emission spectrum with the acceptor detection channel causes some emission of the donor to appear in the **S** image (leak-through; Fig 7.1C), and second, due to overlap of the acceptor excitation spectrum, some acceptors are directly (inappropriately) excited at the donor excitation wavelength (cross-excitation; Fig 7.1C) and this causes acceptor fluorescence independent from FRET. Thus, the first problem is:

> **FilterFRET Problem 1: Spectral overlap**
>
> **S** *is a mixture of sensitized emission, donor- and acceptor fluorescence.*

Even if we forget, for a moment, the overlap problem and assume that we obtained a "pure" sensitized emission image, interpretation of this image is still ambiguous. That is because first, the intensity of **S** varies linearly with the excitation intensity and with the detector sensitivity. The exact same preparation will, when measured on a different microscope, yield different s.e. intensities. In fact, as much as renewing the arc lamp would impede comparison of results obtained on the same microscope. Second, the interpretation

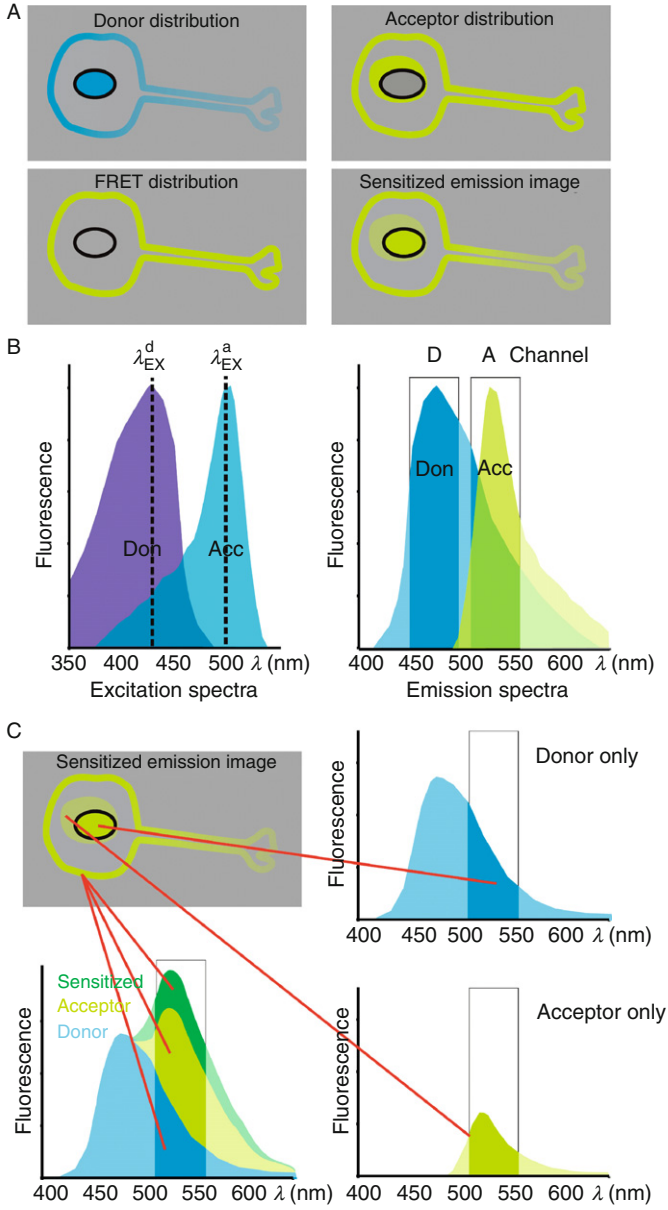

Fig. 7.1. (*Continued*)

of local differences in s.e. within a single image is also ambiguous. For example, the diminished s.e. in the axon of our model neuron (Fig. 7.1C) may either stem from less efficient interaction between donors and acceptors or from locally decreased abundance of donors and/or acceptors. As one often is interested in the distribution of the *degree* of protein interaction, the s.e. image must thus be normalized by relating it to the local concentration of the donor, the acceptor, or both. Thus:

FilterFRET Problem 2: Normalization

S *depends on FRET efficiency but also on fluorophore concentration, donor excitation, and detector sensitivity.*

To perform such normalization, images of the distribution of the donors and acceptors are needed. For the donor image (**D**), donor emission is collected while exciting at donor wavelength, and for the acceptor image (**A**), the acceptor fluorescence is imaged while exciting at acceptor wavelength. Unfortunately, these images also contain components of spectral overlap. In addition, **D** also contains a (negative) component of FRET because inevitably some donor emission will be lost due to resonance. This creates a recurrent problem: we cannot calculate s.e. because we do not know the

Fig. 7.1. *Detecting sensitized emission.* (A) Neuronal cell expressing donors (blue) at the membrane and in the nucleus, and acceptors (green) at the membrane and around the nucleus. Lower abundance of the donor in the axon is also depicted. FRET can only occur at the membrane of this cell (lower left panel). (B) Normalized excitation spectra of donors (CFP) and acceptors (YFP). Indicated are the donor- and acceptor excitation lines (left panel) and the two detection channels (bandpass filters). (C) Appearance of signals in the s.e. image. Whereas FRET is restricted to the membrane, due to leak-through of donor signal in the s.e. channel (e.g., in the nucleus; rightmost spectrum) and false excitation of acceptors (e.g., around the nucleus; lower right spectrum and figure B) additional signals are apparent. Note that leak-through and cross-excitation are not restricted to areas stained with either donors or acceptors alone (lower left panel).

donor distribution, and the reason that we do not know this is that we cannot correct it for the unknown s.e. Similarly, the acceptor levels may not be directly derived from **A** if this image also contains some emission of donor molecules that have been cross-excited at the acceptor excitation wavelength and that bleed into the acceptor channel. It would appear that this latter term is always very small, but as we will see later on in this chapter its contribution may become significant when acceptors are present very sparsely and the sensitivity of the acceptor channel is increased to cope with that fact. Thus:

FilterFRET Problem 3: Reference donor- and acceptor images

Relative donor and acceptor levels cannot be determined directly from **D** *and* **A** *images.*

Once proper corrections have been applied to donor, acceptor, and s.e. images (i.e., Problems 1 and 3 have been tackled), we can proceed with Problem 2 and normalize the data. Here, a final important issue is raised: that of absolute quantification. Let us define here the apparent donor FRET efficiency E_D as the fraction of energy quanta absorbed by all donors (whether in complex with an acceptor or not) in a given pixel that is transferred to acceptors (note the difference with FRET efficiency E as defined in other chapters, which is the chance that excitation of the donor in a *donor–acceptor complex* leads to transfer to the acceptor). By definition, both E_D and E should be corrected, normalized, and quantitative measures for interactions. However, the quantitative E_D cannot be simply obtained by dividing corrected **S** and **D** images because **S** and **D** are not to the same scale. That is, even if **S** and **D** share the same excitation settings (which cancels out excitation changes as a source of variance), **D** and **S** are obtained with different "sensitivity" because filter settings, detector gain, and quantum yields of fluorophores are not the same. To be able to directly compare results obtained in different labs and with different setups, we thus have to find a scaling parameter that relates the sensitivity of the setup for donors to that for acceptors.

FilterFRET Problem 4: Getting it quantitative

Corrected s.e. and donor images are not to the same scale because they have been recorded under different conditions.

Luckily, a mathematical framework to solve these problems has been worked out by several groups [1–6] who showed that from just three acquired images **S**, **D**, and **A** quantitative FRET efficiency images can be calculated. This framework relies on calibrations taken from cells expressing either donors only or acceptors only and it allows direct comparison of results obtained around the world.

Before embarking on a detailed treatment of filterFRET, for completion we will briefly treat earlier nonquantitative FRET imaging methods that rely on calculating the ratio of **S** and either **D** or **A**. While not quantitative, ratio imaging is still widely in use because it is very simple and, depending on the biological application, it often gives enough information to provide answers.

7.2. Two-channel ratio imaging

7.2.1. Emission ratio

Emission ratio imaging is extremely popular due to its simplicity and speed. In essence, cells expressing donors and acceptors are illuminated at the donor wavelength and fluorescence intensity data are collected both at donor (**D**) and at acceptor (**S**) channels. Collected data may be either images, or, in case high acquisition speed is crucial and spatial information is not required, dual-channel photometer readings (see Textbox 1). **S** and **D** are not overlap-corrected and "FRET" is simply expressed as the ratio of intensities[1] as: ratio = **S/D**.

[1]Variations on the simple ratio are also encountered in literature, for example, S/(S + D).

Emission ratioing yields some form of normalization (provided that the FRET efficiency is small) and it nicely cancels out light source intensity fluctuations. It does not, however, provide sufficient data to calculate FRET quantitatively in most cases. Nevertheless, there are cases where quantitative FRET data are not needed to still be able to draw biological conclusions. For example, to study agonist-induced changes in FRET, emission ratio data from time-lapse series provide good information on the time course and localization of the induced FRET changes, and a reasonable impression about the magnitude. In addition, a better quantitative feel for the data can be obtained if endpoint calibrations are applicable, for example, if FRET can be experimentally maximized (see Textbox 1) [7–9].

Ratio imaging is particularly suited for single-polypeptide FRET sensors. In these constructs FRET changes are due to altered distance and/or orientation of the donor and acceptor, and since the fluorophores are tethered their stoichiometry is always fixed. Thus, the filterFRET problems are easier to address and, assuming full maturation of both FPs [4], it can in fact be shown that under these circumstances two images suffice to calculate FRET quantitatively (see Textbox 1 and Appendix 7.A.6).

7.2.2. Excitation ratio

In principle, similar information can be obtained from excitation ratioing where acceptor images are acquired at both donor (**S**) and acceptor (**A**) excitation wavelength, and FRET is apparent from ratio = **S/A**.

Because of the double exposure, the preparation suffers from increased bleaching and photodamage. Furthermore, split-imaging on charge-coupled-device (CCD) systems (see Textbox 1) is not an option. Nevertheless, excitation ratioing may be an economic choice for laboratories that have an old Fura-imaging setup. These microscopes often allow very fast excitation switching

Textbox 1. **Ratio imaging**

Emission ratio imaging involves collection of **S** and **D** images from the preparation. On wide-field microscopes, **D** and **S** can be sequentially acquired by emission filter switching, for example, using a filter wheel. This requires two consecutive exposures, causing unnecessary photobleaching and raising the risk of errors due to cell movements (Fig. 7.T1). Therefore it is better to collect the images simultaneously, for example, using a commercially available image-splitting device (Fig. 7.T1B) that projects the channels on two halves of the same CCD camera chip. Note, however, that these devices require precise calibration to ensure perfect co-registration of the images. On point-scanning confocal microscopes, simultaneous acquisition of **D** and **S** is also possible and the two images will usually overlap quite well.

Ratio imaging nicely cancels out some of the main complications in the interpretation of wide-field images in that it normalizes fluorescence intensity differences caused by for example, cell height (Fig. 7.T1) as well as possible slow drift in excitation intensity. Light sources invariably are much less stable than detectors. Incidentally, for these reasons emission ratio imaging has been applied for over 3 decades by the Ca^{2+} imaging community.

In Fig. 7.T1C, a special case of emission ratioing is shown. Rather than forming an image, the objective is used to project the emission on a beamsplitter/dual-photometer assembly that simply records the total emission in **S** and **D** channels. Pooling of all the emission photons allows for dimming of the excitation intensity by several orders of magnitude, effectively eliminating photodamage. Whereas spatial resolution is given up, this setup is ideally suited for fast kinetic experiments because it can easily be tuned for sub-ms temporal resolution.

(*Continued*)

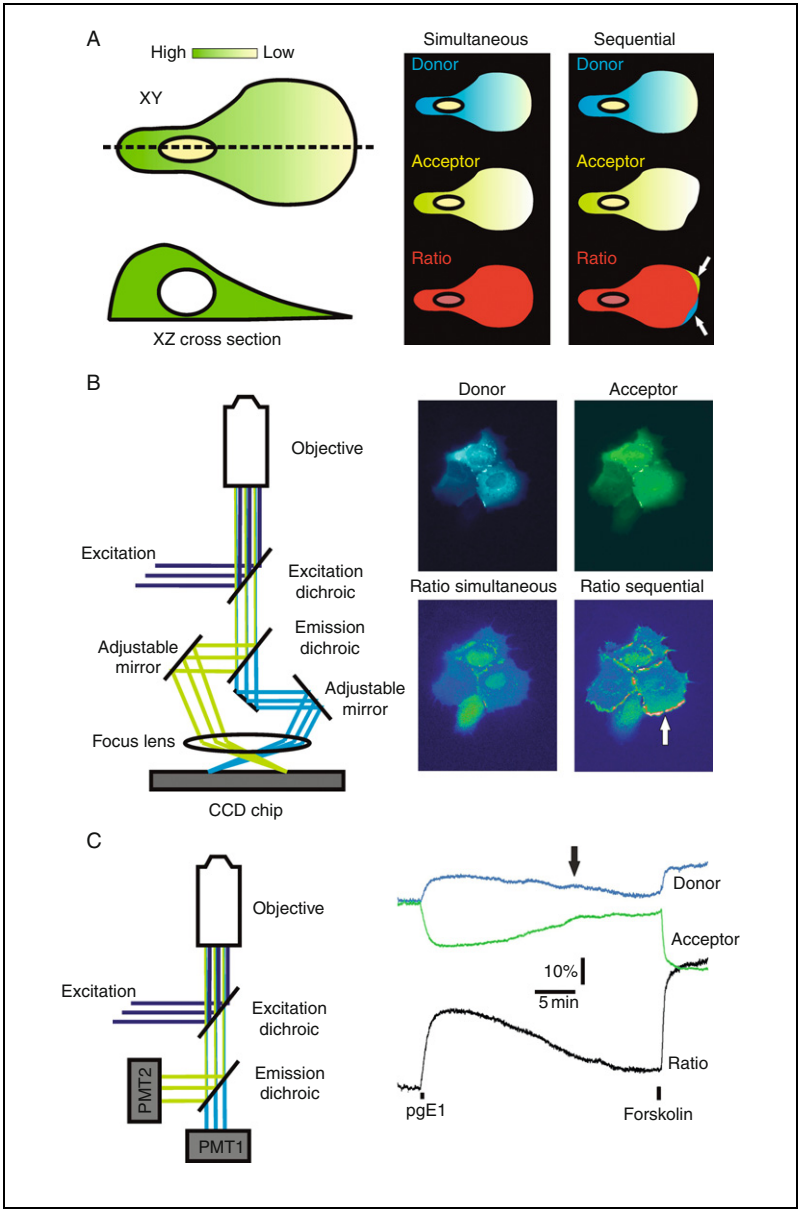

The traces in Fig. 7.T1C show a typical result and also illustrate the use of FRET endpoint calibrations by manipulating the preparation to a state of maximal FRET.

In general, ratio imaging is not quantitative nor is it, strictly spoken, normalized because the acquired data do not permit Problems 1–4 (see Sect. 7.1.1) to be properly addressed. One important exception is the case where donors and acceptors are present at a fixed stoichiometry. Examples of that are the popular single-polypeptide FRET sensors. In this case, the normalization problem (2) is inherently solved and the overlap- and reference-image problems (1 and 3) simplify considerably. It can be shown [1 and Appendix 7.A.6] that in that case FRET efficiency (E) can be calculated from **D** and **S** images.

Fig. 7.T1. *Emission ratio imaging of the cAMP FRET sensor CFP-Epac-YFP* [8]. (A) Ratio imaging largely corrects intensity differences that are due to cell morphology. However, if channels are collected consecutively, any shape changes of the cells cause errors (arrows) in the ratio image that may easily be mistaken for FRET differences. (B). Simultaneous image collection. **D** and **S** are projected side by side on a CCD chip using a commercially available image splitting device fitted to a widefield epifluorescence microscope. The ratio image (lower left photomicrograph) is calculated using Image J; no attempt was made to correct for bleedthrough. The lower right ratio image shows errors due to cell movement (images taken 5 s apart) (C) Emission ratioing using a beam splitter and dual photometer setup. Traces represent **D** (blue), **S** (green), and the ratio (black). Since the Epac sensor looses FRET upon binding to cAMP, in this case the ratio was calculated as **D**/**S** to have upward ratio changes correspond with increased [cAMP]. Note that excitation fluctuations (arrow) disappear in the ratio. All data courtesy of B. Ponsioen.

and may be adapted for FRET by a mere filter change. Furthermore, unlike the emission ratio, the ratio **S**/**A** changes linearly with FRET.

7.3. Three-channel measurements: FilterFRET

In this section, FRET will be calculated from sets of three separately acquired images that are chosen to optimally detect s.e. (**S**), donor emission (**D**), and acceptor emission (**A**). Because both the excitation and emission spectra of donor and acceptor overlap extensively, **S**, **D,** and **A** likely also contain leak-through components that have to be subtracted (Fig. 7.2). Just how much leak-through needs to be subtracted depends on calibration values that must be calculated from measurements obtained with special reference samples. Note that in essence our treatment follows and builds on the work of several authors [1–3, 5, 6, 10–12]. Most of the published correction schemes have been worked out for images acquired with a wide-field fluorescence microscope equipped with digital camera [1, 2, 5, 6, 10]; however, a variety of mathematical terminologies has been used. For confocal images, we showed that correction is distinctly more complex because the sensitivities of the detection channels are varied independently [3]. We here present a generalized mathematical framework, with an attempt to arrive at a compromise in terminology.

7.3.1. Sensitized emission

In the following treatment it is assumed that detector gain and offset are correctly adjusted, and that autofluorescence of cells is either negligible or properly subtracted. In addition, it is assumed that the images are shading-corrected; see Sect. 7.4.4. For details on shading techniques, the reader is referred to Nagy et al. and Tomazevic et al. [10, 13]. Provided that independent measurements on the magnitude of cross talk terms can be made, straightforward corrections can be carried out from three acquired images:

- Donor excitation with donor emission, **D**
- Donor excitation with acceptor emission, **S**
- Acceptor excitation with acceptor emission, **A**

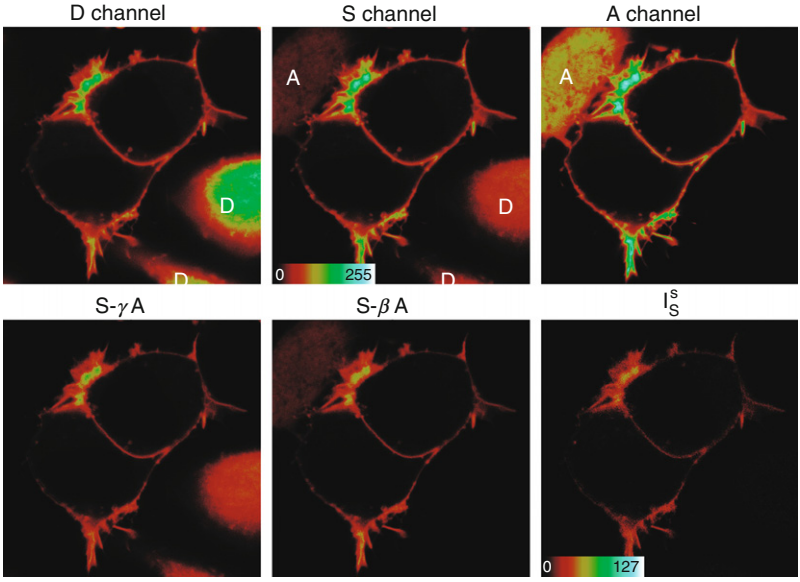

Fig. 7.2. *Sensitized emission calculated from confocal images*. Cells expressing CFP- and YFP-tagged Pleckstrin homology (PH) domains were seeded together with control cells expressing either CFP (marked "D") or YFP (marked "B"). Top row shows raw input files and illustrates donor leak-through (middle panel, "D") and cross-excitation (middle panel, "A"). In the bottom row, **S** images are corrected for cross-excited YFP (left), for CFP leak-through (middle) or according to Eq. (7.8) (right panel). The contrast of the I^s_S panel is stretched twofold as indicated. All images in this chapter are collected with Leica TCS SP2 or SP5 confocal microscopes except for Fig. 7.T1, which was acquired with a Leica ASMDW wide-field epifluorescence microscope equipped with dual-view adapter (Optical Insights). Image acquisition and specimen refocusing were automated from within a custom-made Visual Basic (v6.0) program by calling commands from the Leica macro tool package. ROIs were manually assigned to cells expressing only CFP or YFP and from these, correction factors were measured and calculated. Using these factors, sensitized emission was calculated as outlined in the text.

The acquired images are composite images that consist of fluorescence stemming from different molecular species: donors, acceptors, or FRET pairs (Figs. 7.1 and 7.2). These fluorescent

components are denoted by I (intensity) followed by a capitalized subscript ($_D$, $_A$, or $_S$, for respectively donors, acceptors, or donor/acceptor FRET pairs) to indicate the particular population of molecules responsible for emission of I, and a lower-case superscript ($^{d,\ a,}$ or ^{s}) that indicates the detection channel (or filter cube). For example, I_D^{d} denotes the intensity of the donors as detected in the donor channel and reads as "Intensity of donors in the donor channel," etc. (see Table 7.1).

The terms in the composite images thus are as follows:

- **D** is the sum of the remaining donor fluorescence in the donor channel $\left(I_{D-S}^{\mathrm{d}}\right)$, and of leak-through components of sensitized emission back into the donor channel $\left(I_S^{\mathrm{d}}\right)$ and of cross-excited acceptors back into the donor channel $\left(I_A^{\mathrm{d}}\right)$.

$$\mathbf{D} = I_{D-S}^{\mathrm{d}} + I_S^{\mathrm{d}} + I_A^{\mathrm{d}} \tag{7.1}$$

- **S** contains energy transfer $\left(I_S^{\mathrm{s}}\right)$, leak-through from the "donor minus FRET" population $\left(I_{D-S}^{\mathrm{s}}\right)$ and emission from cross-excited acceptors $\left(I_A^{\mathrm{s}}\right)$.

$$\mathbf{S} = I_{D-S}^{\mathrm{s}} + I_S^{\mathrm{s}} + I_A^{\mathrm{s}} \tag{7.2}$$

- Finally, **A** contains acceptor fluorescence $\left(I_A^{\mathrm{a}}\right)$ and two usually very minor leak-through components: that of the (partially quenched) donor population inappropriately excited at acceptor wavelength and leaking into the acceptor channel $\left(I_{D-S}^{\mathrm{a}}\right)$, and the small amount of sensitized emission that stems from FRET after inappropriate excitation of donors at acceptor wavelength $\left(I_S^{\mathrm{a}}\right)$.

$$\mathbf{A} = I_{D-S}^{\mathrm{a}} + I_S^{\mathrm{a}} + I_A^{\mathrm{a}} \tag{7.3}$$

In the majority of cases, the two cross-terms in this equation can be ignored (i.e., are $\ll 0.01$) and Eq. (7.3) simplifies to:

$$\mathbf{A} = I_A^{\mathrm{a}} \tag{7.3'}$$

TABLE 7.1
Glossary of terms

Symbol	Excitation	Emission	Fluorophore	Indicates
D	Don	Don		raw donor image collected at λ_{ex}^{d} with donor emission filter (donor channel)
S	Don	s.e.		raw sensitized emission image collected at λ_{ex}^{d} with the sensitized emission filter (s.e. channel)
A	Acc	Acc		raw acceptor image collected at λ_{ex}^{a} with the acceptor emission filter (acceptor channel)
I_D^d	Don	Don	Don	unquenched donor signal in the donor channel
I_S^d	Don	Don	s.e.	(acceptor) s.e. leaking through in the donor channel
I_A^d	Don	Don	Acc	cross-excited (at λ_{ex}^{d}) acceptor emission leaking through in the donor channel
I_D^s	Don(S)[1]	s.e.[2]	Don	leak-through of unquenched donor excited at λ_{ex}^{d} in s.e. channel
I_S^s	Don(S)	s.e.	s.e.	(acceptor) s.e. signal detected in the s.e. channel
I_A^s	Don(S)	s.e.	Acc	emission of acceptors cross-excited at λ_{ex}^{d} in the s.e. channel
I_D^a	Acc	Acc	Don	cross-excited (at λ_{ex}^{a}) signal of unquenched donors leaking through in the acceptor channel
I_S^a	Acc	Acc	s.e.	(acceptor) s.e. in acceptor channel at λ_{ex}^{a}; this signal derives from the small population of cross-excited donors that leads to FRET

(*Continued*)

TABLE 7.1 (*Continued*)

Symbol	Excitation	Emission	Fluorophore	Indicates
I_A^a	Acc	Acc	Acc	(directly excited) acceptor signal in the acceptor channel
I_{D-S}^d	Don	Don	Don[3]	(partly) quenched donor signal in the donor channel
I_{D-S}^s	Don(S)	s.e.	Don[3]	leak-through of the (partly) quenched donor signal in the s.e. channel
I_{D-S}^a	Acc	Acc	Don[3]	leak-through of the cross-excited, (partly) quenched donor signal in the s.e. channel

The fluorescent components are denoted by I (intensity) followed by a capitalized subscript ($_{D,\,A,}$ or $_S$, for respectively Donors, Acceptors, or s.e.) to indicate the particular population of molecules responsible for emission and a lower-case superscript ($^{d,\,a,}$ or ^{s}) that indicates the detection channel (or filter cube). For example, I_D^d denotes the intensity of the donors as detected in the donor channel and reads as "Intensity of donors in the donor channel," etc. Notes: (1) The excitation in the s.e. channel is generally set up to be equal to that in the donor channel. In case a separate filter cube is used, slight differences may occur, which is denoted by Don(S). See the text and appendix for further details. (2) The s.e. emission filter is usually the same as the acceptor emission filter in confocal determinations. We here designate a different filter to accommodate those wide-field/digital camera experiments that employ different filters for A and S. (3) Here the notation D–S indicates the residual (quenched) donor fluorescence in the presence of the acceptor. In the other chapters this is indicated as DA. Hence: $I_{D-S}^d = I_{DA}^d$; $I_{D-S}^s = I_{DA}^s$; and $I_{D-S}^a = I_{DA}^a$.

For those cases where cross-terms cannot be ignored, we derive an expression in Sect. 7.A.5.

Now, note that each of the leak-through terms in Eqs. (7.1) and (7.2) is just a fixed fraction of the intensity in its "own" channel:

$$I_A^d = \alpha I_A^a \ (= \alpha A) \tag{7.4}$$

$$I_{D-S}^s = \beta I_{D-S}^d \tag{7.5}$$

$$I_A^{\mathrm{s}} = \gamma I_A^{\mathrm{a}} \ (= \gamma A) \tag{7.6}$$

$$I_S^{\mathrm{d}} = \delta I_S^{\mathrm{s}} \tag{7.7}$$

where α is the ratio of pure acceptor fluorescence detected using donor/acceptor filters, β is the leak-through of pure donor fluorescence in the acceptor (s.e.) channel, δ that for leak-through of sensitized emission back into the donor channel, and γ relates acceptor fluorescence excited at donor wavelength and detected in the s.e. channel to the acceptor fluorescence excited at acceptor wavelength and detected in the acceptor channel. Further, it can be easily shown that $\alpha = \gamma\delta$ (see Textbox 2 and Appendix).

We can thus rewrite Eqs. (7.1) and (7.2) to:

$$\mathbf{D} = I_{D-S}^{\mathrm{d}} + \delta I_S^{\mathrm{s}} + \gamma\delta\mathbf{A} \tag{7.1B}$$

$$\mathbf{S} = \beta I_{D-S}^{\mathrm{d}} + I_S^{\mathrm{s}} + \gamma\mathbf{A} \tag{7.2B}$$

which rearranges to [3]:

$$I_S^{\mathrm{s}} = \frac{\mathbf{S} - \beta\mathbf{D} - \gamma(1 - \beta\delta)\mathbf{A}}{1 - \beta\delta} \tag{7.8}$$

Sensitized emission $\left(I_S^{\mathrm{s}}\right)$, as defined in Eq. (7.8), reliably measures the *relative* amount of energy transfer occurring in each pixel (Fig. 7.2, lower right panel). I_S^{s} is corrected for spectral overlap (i.e., Problem 1 has been taken care of); however, unlike E, it is not a normalized measure for interaction nor is it quantitative in absolute terms. It depends on the specific biological question which of the two yields the most relevant information.

7.3.2. FRET efficiency

Having obtained the s.e. image I_S^{s}, which provides a spatial map of molecular interactions in the cell, the next steps are normalization and absolute quantification of the interactions. Normalization can

Textbox 2. **The leak-through parameters**

The correction factors α, β, γ, and δ must be determined independently. From Eqs. (7.4) to (7.7), it is clear that estimates for α, γ, and δ can be obtained by imaging a sample with only acceptor molecules and calculating:

$\alpha = \mathbf{D}/\mathbf{A}$ leak-through of cross-excited acceptors back into the donor channel
$\gamma = \mathbf{S}/\mathbf{A}$ cross excitation of acceptors
$\delta = \mathbf{D}/\mathbf{S}$ leak-through of s.e. back into the donor channel

Similarly, β is estimated from a sample with only donor molecules:

$\beta = \mathbf{S}/\mathbf{D}$ leak-through of donors into the s.e. channel

Note that parameters β and δ depend on signal amplifications in the utilized detectors and on the elements in the optical path (optical filter, spectral detection bands) only, while α and γ are additionally influenced by relative excitation intensity. This is usually a fixed constant in wide-field microscopy but in confocal imaging laser line intensities are adjusted independently. Furthermore, note that the α factor equals δ multiplied by γ (see Appendix for further detail).

be carried out through division of the s.e. image by a pure donor image to arrive at the "*apparent* FRET efficiency" (not to be confused with the quantitative E_D):

$$^{\text{app}}\text{FRET}_D = I_S^{\text{s}}/I_D^{\text{d}} \tag{7.9}$$

where the denominator represents the total donor fluorescence as it would appear in the absence of FRET. That is, the pure donor image in the denominator has to be corrected for leak-through components and for loss of donor emission due to FRET (Problem 3) [1, 3, 5, 6].

Sometimes normalization to the acceptor image is encountered:

$$^{\text{app}}\text{FRET}_A = I_S^{\text{s}}/I_A^{\text{a}} \tag{7.10}$$

This is easier because the acceptor image is readily available (Eq. (7.3′)) without further corrections. $^{\text{app}}\text{FRET}_A$ and $^{\text{app}}\text{FRET}_D$ are not quantitative in that nominator and denominator images are acquired in different channels. Thus, their relative magnitude depends on filter settings, detector gain, on donor and acceptor quantum yield and, in the case of $^{\text{app}}\text{FRET}_A$, also on relative excitation intensities. While neither $^{\text{app}}\text{FRET}_A$ nor $^{\text{app}}\text{FRET}_D$ solve the problem of quantification, both are frequently encountered in the literature and both do allow quantitative comparison of interactions *within the same image*.

In order to obtain the desired quantitative measure of FRET (Fig. 7.3), an additional correction factor must scale the nominator to the denominator in Eq. (7.9) [1–3, 6]. In other words, we must relate the FRET-induced sensitized emission in the **S** channel to the loss of donor emission in the **D** channel as in:

$$E_D = \frac{\text{Loss in donor emission due to FRET}}{\text{Total donor emission in the absence of FRET}} \tag{7.11}$$

or in our terminology:

$$E_D = \frac{I_D^{\text{d}} - I_{D-S}^{\text{d}}}{I_D^{\text{d}}} = 1 - \frac{I_{D-S}^{\text{d}}}{I_D^{\text{d}}} \left(= 1 - \frac{I_{DA}}{I_D} \right) \tag{7.11A}$$

Note that the "*Loss in donor emission due to FRET*" (Eq. (7.11)) is just a constant times the "*sensitized emission*" (Eq. (7.8)) for given acquisition settings, or $I_{\text{Loss}}^{\text{d}} = \phi I_S^{\text{s}}$. Thus (noting that both $I_{\text{Loss}}^{\text{d}}$ and ϕ have negative values):

$$I_{D-S}^{\text{d}} = I_D^{\text{d}} + I_{\text{Loss}}^{\text{d}} = I_D^{\text{d}} + \phi I_S^{\text{s}} \tag{7.12}$$

Now it is straightforward to solve for I_D^{d} and I_{D-S}^{d}. Substituting Eq. (7.12) in Eq. (7.2B), **S** and **D** become:

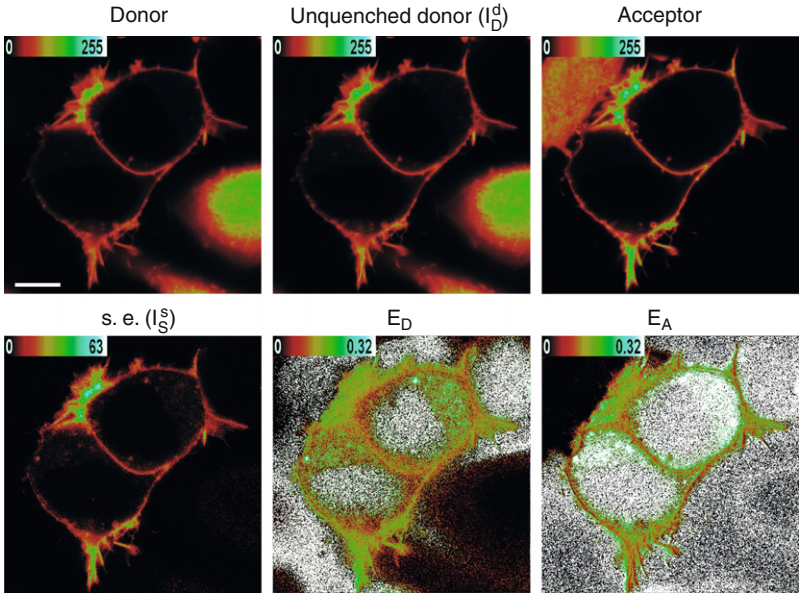

Fig. 7.3. Fret efficiency. The unquenched donor image (top row, middle panel), as calculated according to Eq. (7.13), and the acceptor image (top right panel) are used to normalize the s.e. image. The resulting images E_D and E_A (Eqs. (7.10) and (7.11), respectively) are quantitative, as detailed in the text. Unfiltered, raw data are shown. Scale bar is 12 μm.

$$\mathbf{D} = I_D^{\mathrm{d}} + (\phi + \delta) I_S^{\mathrm{s}} + \gamma\delta\mathbf{A} \tag{7.1C}$$

$$\mathbf{S} = \beta I_D^d + (\beta\phi + 1) I_S^s + \gamma\mathbf{A} \tag{7.2C}$$

Combining Eqs. (7.8) and (7.1C):

$$I_D^{\mathrm{d}} = \frac{\beta\phi + 1}{1 - \beta\delta}\mathbf{D} - \frac{\phi + \delta}{1 - \beta\delta} S + \gamma\phi\mathbf{A} \tag{7.13}$$

defining

$$\zeta = \frac{\beta(\phi + \delta)}{1 - \beta\delta} \tag{7.14}$$

then:

$$I_D^{\mathrm{d}} = (\zeta + 1)\mathbf{D} - \frac{\zeta}{\beta}\mathbf{S} + \gamma\left(\delta - \frac{\zeta}{\beta} + \delta\zeta\right)\mathbf{A} \tag{7.13B}$$

Note that this equation is identical to the expression for unquenched donor fluorescence of van Rheenen et al. (Eq. (A17)).

And for I_{D-S}^{d} we can derive the following expression after combining Eqs. (7.1B) and (7.2B):

$$I_{D-S}^{\mathrm{d}} = \frac{\mathbf{D} - \delta\mathbf{S}}{1 - \beta\delta} \tag{7.15}$$

Thus, we now have the results to express E_D as:

$$E_D = 1 - \frac{I_{D-S}^{\mathrm{d}}}{I_D^{\mathrm{d}}} = 1 - \frac{\mathbf{D} - \delta\mathbf{S}}{(\beta\phi + 1)\mathbf{D} - (\delta + \phi)\mathbf{S} + \phi(1 - \alpha\beta)\mathbf{A}} \tag{7.16}$$

7.3.3. Making it quantitative

One final step is needed to wrap things up: the factor ϕ (which relates the s.e. in **S** to loss of donor fluorescence in **D**) that was introduced to solve for I_D^{d} must be determined. Note that for a given combination of filter settings and fluorophores ϕ is a constant, independent from expression levels and excitation intensity. For the popular cyan fluorescent protein (CFP)/yellow fluorescent protein (YFP) FRET pair, we have mostly used a very intuitive approach that employs Yellow Cameleon, the well-known single-polypeptide intracellular Ca^{2+} sensor. This construct shows significant FRET change upon raising intracellular Ca^{2+} concentration with, for example, ionomycin [7]. Recording **D** and **S** before and after ionomycin-induced Ca^{2+} saturation of Yellow Cameleon gives paired observations for Eqs. (7.1C) and (7.2C) that differ only in FRET efficiency. The increase in **S** is:

$$\begin{array}{l} \mathbf{S}(\text{post}) = \beta I_D^{\text{d}} + (\beta\phi + 1) I_S^{\text{s}}(\text{post}) + \gamma \mathbf{A} \\ \mathbf{S}(\text{pre}) \;\; = \beta I_D^{\text{d}} + (\beta\phi + 1) I_S^{\text{s}}(\text{pre}) \;\; + \gamma \mathbf{A} \\ \hline \mathbf{S}(\text{post}) - \mathbf{S}(\text{pre}) = (\beta\phi + 1)\left(I_S^{\text{s}}(\text{post}) - I_S^{\text{s}}(\text{pre})\right) \end{array} \text{subtract} \quad (7.17)$$

And for the change in D:

$$\begin{array}{l} \mathbf{D}(\text{pre}) \;\; = I_D^{\text{d}} + (\delta + \phi) I_S^{\text{s}}(\text{pre}) \;\; + \gamma\delta \mathbf{A} \\ \mathbf{D}(\text{post}) = I_D^{\text{d}} + (\delta + \phi) I_S^{\text{s}}(\text{post}) + \gamma\delta \mathbf{A} \\ \hline \mathbf{D}(\text{pre}) - \mathbf{D}(\text{post}) = -(\delta + \phi)\left(I_S^{\text{s}}(\text{post}) - I_S^{\text{s}}(\text{pre})\right) \end{array} \text{subtract} \quad (7.18)$$

Dividing Eq. (7.17) by Eq. (7.18) gives:

$$\frac{\mathbf{S}(\text{post}) - \mathbf{S}(\text{pre})}{\mathbf{D}(\text{pre}) - \mathbf{D}(\text{post})} = -\frac{\beta\phi + 1}{\phi + \delta} \equiv G \quad (7.19)$$

or[2]

$$\phi = -\frac{1 + \delta G}{\beta + G} \quad (7.20)$$

Note that G as derived here relates the FRET-induced sensitized emission in the **S** channel to the loss of donor emission in the **D** channel and that it is identical to the correction factor γ/ξ [2] or G [6, 14]. Note however, that if the correction factors β or δ change, G and ϕ change as well. In contrast, our correction factor ζ [3] is a constant that depends only on fluorophore properties and filter settings, and therefore it does not change with excitation intensity or detector gain. This is a clear advantage for confocal filterFRET. ζ (Eq. (7.14)) and G (Eq. (7.19)) are related as:

$$G = -\beta\left(1 + \frac{1}{\zeta}\right) \quad (7.21)$$

[2]Note that we have slightly rearranged the math from van Rheenen et al, BJ 2004 to adopt the correction factor G that is used in several publications.

and

$$\zeta = -\frac{\beta}{\beta + G} \tag{7.22}$$

Of course any of the many cytosolic constructs that can be forced to change FRET are useful for calibration, as long as the fluorophores are the same as those used in the experiments. We have for example also successfully used caspase-cleavable GFP-mRFP chimera (unpublished results).

Several other approaches to solve the quantitation problem have been proposed. Hoppe et al. [2] determined γ/ξ by calibrating it against constructs with known FRET efficiency. We and others [3, 6] have used data from a cell before and after acceptor photobleaching to relate the FRET-induced sensitized emission in the **S** channel to the loss of donor emission in the **D** channel by factors termed ζ or G, respectively. For the CFP/YFP pair this works very well on confocal microscopes with a 514-nm Argon ion laser line, but on wide-field systems, selective acceptor photobleaching reportedly causes problems [14]. Finally, G can also be determined by comparison of several constructs that differ in FRET efficiency, a bit analogous to the Yellow Cameleon calibration described above [10, 14].

7.3.4. Stoichiometry

The FRET efficiency E_D as determined above is the fraction of energy quanta absorbed by all donor molecules that is transferred to acceptors. For a given pixel, E_D effectively reflects both the efficiency with which paired donor–acceptors transfer energy (E) and the fraction of molecules in that pixel that pair up (f_D). This means, for example, that a pixel with $E_D = 0.2$ may result from 100% of donors having $E = 0.2$, or from 20% of donors having $E = 1$, or anything in between. The FRET efficiency E of a donor/acceptor pair (termed characteristic FRET efficiency, E_c in some literature [2, 3]) is most often unknown.

However, if a good estimate of E can be made, the fraction of donors in complex can be readily calculated as

$$f_D = \frac{E_D}{E} \tag{7.23}$$

The cases where reliable determination of E is possible are those where good assumptions can be made based on known fluorophore dipole alignment and distance and those where the donors and acceptors can be induced to quantitatively engage in interactions (for example, by determining FRET in an (in vitro) preparation of a 1:1 donor–acceptor mix, or by inducing maximal interaction in a single-polypeptide FRET sensor such as Yellow Cameleon or CFP-Epac-YFP, see Figure in Textbox 1). In vivo, usually many uncertainties exist that prevent determination of E. For example, distance and orientation of donors and acceptors may be variable and FRET may also occur between molecules that just happen to come within resonance range (sometimes called spurious- or collision FRET). This latter effect is very small for molecules in solution, but it dramatically increases when the donors and acceptors are concentrated in cell organelles. For example, even donor- and acceptor-tagged molecules that are distributed randomly (i.e., not clustered) at the membrane will yield significant FRET despite moderate expression levels (for analysis, see Appendix of van Rheenen et al. [15]). Thus, E_D reflects both intra- and inter FRET-pair resonance, and consequently f_D would be overestimated (which incidentally also holds true for the determination of E or f_D using FLIM). Usually I_S^s, E_D, and E_A can be reliably determined, but in the vast majority of FilterFRET or FLIM experiments E and f_D will be unknown.

Unlike donor-based FRET methods like FLIM, filterFRET also yields spatial information on the acceptor population. This means that in addition to querying donor-FRET (by solving for E_D or I_D^d), we can also assess the relationship between sensitized emission and the acceptor population. At 1:1 stoichiometry obviously E_D should equal the acceptor-normalized efficiency E_A. In other cases, E_A deviates from E but sometimes can yield biologically more relevant information than E_D or E. For example, dislocation of 50% of the

donors from an organelle decorated with donor–acceptor pairs into the cytosol might leave 50% of acceptors unpaired at the organelle. E_D would in this case report that the remaining 50% donors still interact just as efficiently, whereas E_A clearly reveals the lowered acceptor occupation by dropping with 50%.

What is the donor/acceptor ratio in a given cell? Again, this ratio cannot be directly derived because it concerns two quantities that stem from fluorophores with different properties (absorption coefficient, quantum yield, spectra) and that emit into two channels differing in gain, filters, and excitation intensity. Thus, the (overlap corrected) intensity of acceptors in channel **A** will be a factor k times that of donors in D, at equimolar concentrations,[3] or:

$$kI_A^{\mathrm{a}} = I_D^{\mathrm{d}} \tag{7.24}$$

For a first approximation, k can be simply calculated by dividing I_D^{d} by I_A^{a} for a donor–acceptor fusion construct, because both quantities are corrected for overlap and FRET. Note however that this requires ϕ to be known (see Sect. 7.3.3). For the ratio of donor to acceptor concentration, we simply find:

$$\frac{[\mathrm{donor}]}{[\mathrm{acceptor}]} = k\frac{I_D^{\mathrm{d}}}{I_A^{\mathrm{a}}} \tag{7.25}$$

Or, in the case of confocal acquisition[4]

$$\frac{[\mathrm{donor}]}{[\mathrm{acceptor}]} = \gamma\sigma\frac{I_D^{\mathrm{d}}}{I_A^{\mathrm{a}}} \tag{7.25B}$$

[3]Termed k in [1]; α in [10]; R in [7], $\kappa\gamma$ in [17].

[4]For confocal imaging with tunable gains, k is not constant. Rather, we can distinguish a fixed part (which relates the efficiency of donor excitation at donor wavelength to that of acceptor excitation at acceptor wavelength) and a part that depends on relative excitation intensities and gains. The former was termed κ in van Rheenen et al. [3] but to keep κ in line with the terminology used in this volume that factor will here be renamed to σ, such that $k = \gamma\sigma$. Also, see Appendix.

Of actual interest to the biologist is usually not the quantification of donor, acceptor, and donor–acceptor, but rather to estimate the concentrations of the interacting proteins and the extent of their interactions, regardless of their labeling state. It is obvious that if the interacting proteins are incompletely labeled (for example, due to the presence of an endogenous population of untagged proteins, or due to imperfect maturation of FP labels) FRET recordings will significantly underestimate the amount of interactions between the proteins. Formalisms to cope with incomplete labeling have been put forward by several groups [2, 4, 16].[5] Inasmuch as such formalisms rely on calibration using donor–acceptor tandem constructs, it is important to note that we observed that speed of maturation of a given FP may dramatically vary from construct to construct [17].

7.4. Optimizing image acquisition

As the I_S^s, E_D, and E_A images are calculated from the raw input images, it is extremely important that **D**, **S,** and **A** are of the best possible quality. In addition, care must be taken that correction factors are derived from reference images taken at exactly the same

[5]Wlodarczyk and coworkers consider that labeling may be incomplete for 2 two reasons: first, not all proteins may become labeled (either in the chemical crosslinking process, or in the case of FP-labeling, due to the presence of endogenous proteins), and second, existing labels may be non-fluorescent, for example due to poor maturation of FPs, or due to photobleaching. Be p_d and p_a the probability that a given molecule of type a and d receive a functional label, respectively, then the concentration of fluorescent donors equals p_d times the total concentration of d plus $(1–p_d)$ times the concentration of complexes, or, in their terminology,

$[D] = p_d.[d] + (1–p_a)[da]$. Analogously,
$[A] = p_a.[a] + (1–p_d)[da]$ and
$[AD] = p_d p_a[da]$.

Provided that proper estimates of p_a and p_d are present, quantitative estimates of interactions can be readily achieved for certain types of experiments.

imaging conditions. In this part, possible pitfalls will be discussed and strategies to improve image quality will be lined out.

7.4.1. Wide-field versus confocal FilterFRET: A comparison

FRET imaging differs enough between wide-field fluorescence microscopes and confocal microscopes to warrant a comparison of the two techniques in this chapter. Confocal imaging offers significant advantages over wide-field imaging because it produces crisp optical sections of the preparation. Furthermore, point-scanning confocals offer greater freedom in image acquisition by allowing free choice of zoom and resolution and independent tuning of channel sensitivities through adjustment of the voltage of the photomultiplier tubes (PMTs). Confocal imaging is also more easily combined with acceptor photo bleaching and with fluorescence recovery after photobleaching (FRAP) experiments. On the other hand, wide-field fluorescence setups offer the freedom to filter-select whatever excitation wavelength desired, and the CCD detectors are more sensitive than PMTs. CCD imaging also is less harsh for the cells than laser point-scanning, although careful tuning of the confocal excitation regime can remedy that for a large part.

These differences have important consequences for filterFRET imaging. The major complication posed by confocal acquisition is that relative sensitivities for **D**, **S**, and **A** are tunable. This is true even if identical filter and pinhole settings are used from experiment to experiment since in general the user wants to fine-tune the excitation line intensities and to control individual PMT gain (high voltage) and offset settings for the channels. With CCD acquisition, weaker fluorescent cells are imaged by increasing the integration time, which causes both I_D^{d}, I_S^{s}, and I_A^{a} as well as the leak-through terms to increase linearly. As a result, when leak-through factors for particular fluorophores and a particular filter set have been quantified once, alterations in integration time can be easily compensated for. In the confocal case, however, unless laser

intensity and PMT settings are kept fixed, this is not possible, due to the nonlinear dependence of gain and offset on the PMT high voltage. This necessitates that β, γ, and δ are determined after each change in setting. The advantage—on the other hand—is that the added flexibility allows simultaneous optimized acquisition of the often weak FRET signals without compromising acquisition time.

Because on CCD setups excitation for **D**, **S**, and **A** images is usually filter-selected from a single white light source the relative intensity of excitation is approximately fixed. Confocal microscopes use separate laser lines, often from distinct lasers, that can (and for optimal imaging should) be independently adjusted. Thus, on CCD setups γ (Eq. (7.6)) is constant for a given set of filters whereas on the confocal, it varies from image to image (also, see Sect. 7.4.2).

A final distinction is that on confocal microscopes **S** and **A** images are commonly acquired with the exact same emission filter settings whereas for CCD microscopes they typically involve physically separate- and therefore slightly different—filter cubes.[6] This simplifies the calculation of leak-through terms [3]. In Appendix of this chapter, we rather generalized the treatment of filterFRET by not making assumptions on the filter settings for **S** and **A**.

These differences add up to one major distinction: on wide-field imaging setups, it suffices to calibrate the setup *just once* for a given set of filters and fluorophores, and then use it for weeks or months without bothering about it. In contrast, for confocal filterFRET imaging, calibrations must be made every time a gain setting or laser line is adjusted, and preferably, for every image.

7.4.2. Temporal errors: Laser intensity fluctuation

On a variety of confocal microscopes, we and others [3, 18] observed considerable drift as well as oscillations (on a time scale of

[6]Unless a dual-excitation filter cube is used, in combination with a excitation switcher.

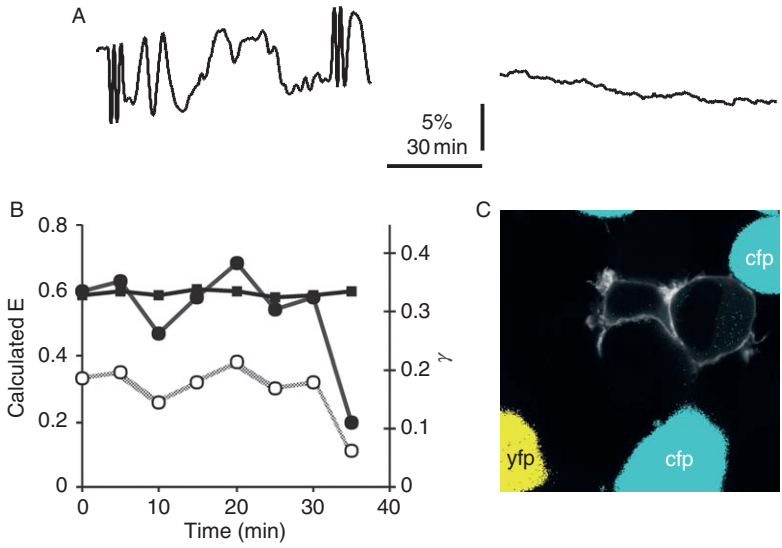

Fig. 7.4. *Correcting excitation fluctuations by inclusion of reference cells.* (A) Fluctuations in the intensity of a 514-nm argon ion laser line (left) and a mercury arc lamp (right), measured every 20 s for a 3 h time period. (B) Calculated E_D (solid circles; left axis) is seen to fluctuate significantly in time-lapse experiments. After 30 min a large intensity fluctuation in acceptor excitation was simulated by manually diminishing laser power with 60%. The open circles depict the correction factor γ, calculated according to Eq. (7.6) from cells expressing acceptors only. Calculating E_D with the online-updated γ-factor (solid squares) abolished the effects of excitation fluctuations. (C) Preparation containing FRET cells (gray) and CFP- and YFP reference cells (blue and yellow), as recognized by automated segmentation based on the ratio of intensity of donors and acceptors.

one to a few minutes) in excitation line intensity (Fig. 7.4A). Changes of several percent are common, while worst-case variations of up to 20% were found in poorly aligned systems. Importantly, individual laser lines fluctuate independently, even when derived from the same laser. Excitation stability is extremely important because it influences γ. While intensity variations may also occur in arc lamps on wide-field fluorescence microscopes, these changes are often much smaller (compare Fig. 7.4 A left and right

panels). Furthermore, slow arc lamp intensity variations affect **D**, **S,** and **A** to the same degree if images are gathered in rapid succession, and thus have no effect on the apparent FRET image (Eqs. (7.9) and (7.10)).

The independent variations in laser line intensity on confocal systems pose a major problem for time-lapse FRET measurements. The supplier of our TCS-SP2 confocal installed a stabilization loop that improved the stability considerably, but not completely. In particular when expected FRET signals are a small fraction of the total fluorescence, the realized stability of ~3% will prevent acquisition of meaningful results. We therefore implemented online correction by recalculating the leak-through factors α, β, γ, and δ for each image [3], as well as G or ϕ (Eqs. (7.4)–(7.19)). To this goal, the cells under study are plated together with a mix of cells expressing either donors or acceptors on the same cover slip (Figs. 7.2 and 7.3). In an image taken at low zoom factor, regions of interest (ROIs) are assigned to single donor- or acceptor transfected cells (Fig. 7.4B and C). Then correction factors are determined from these ROIs as detailed in Eqs. (7.4)–(7.7). E_D and s.e. images are thus calculated using correction factors taken simultaneously with (or just before, in case one wants to zoom in) the FRET cell. This procedure completely removes the effect of laser fluctuations, resulting in superior registration of FRET during acquisition of time-lapse series.

As an alternative, changes in relative intensity of the laser lines may be directly recorded using for example, reflection images or a transmission detector, and γ may be adjusted accordingly. In our experience, this works significantly less reliable.

7.4.3. Co-registration of the input images

Obviously, it is of the utmost importance that the three input channels spatially overlap tightly, both in lateral and in axial direction. Co-registration (i.e., the precise, pixel-by-pixel correspondence of

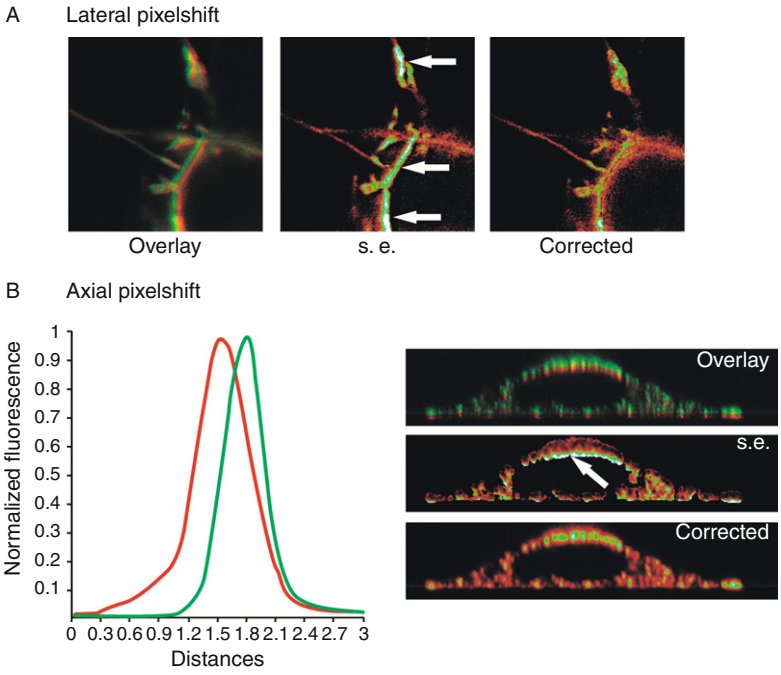

Fig. 7.5. *Effects of poor co-registration on calculated FRET images*. (A) Typical artifacts due to improper alignment (left) of raw input images caused by switching between unmatched filter cubes. The consistent appearance of high FRET values at the right side of bright structures (middle) is a sure indication to check image alignment. Right panel, proper alignment of the images corrects FRET artifacts. (B) Left panel, profiles of fluorescence intensities in a confocal X/Z image of the green emission (525 nm) of a 0.17-microm bead was registered using a HCX PL APO CS 63× objective upon 430-nm (blue line) and 514-nm (red line) excitation. Both scans use detection at 525 nm, demonstrating the extent of axial offset. Right panels, confocal images were acquired from a cell expressing CFP- and YFP-tagged membrane anchors. Top image, green–red overlay illustrates axial offset. Erroneous values (middle image) in the calculated I_S^s (s.e.) image are effectively corrected by using the refocusing macro routine (lower image). Shown are extreme examples.

D, **S,** and **A**) has to be checked meticulously by the experimenter, using for example, color overlay images (Fig. 7.5A). Pixel-shift deviations are common on CCD imaging setups where they are

caused by slight differences in filter cube alignment. When image-splitting devices are used, extensive adjustment for optimal co-registration is always necessary. In contrast, lateral overlay of confocal channels should be excellent for a well-maintained instrument. If needed, co-registration of channels can be easily optimized postacquisition by software pixel-shift algorithms.

Axial co-registration is also important, although it is often completely ignored. Compared with wide-field microscopy, possible focusing deviations (deviations due to offset of donor- and acceptor images in the axial direction) are emphasized by the confocals inherent optical sectioning. When the input images are effectively taken from slightly different planes in the cell, erroneous results occur during calculation of the sensitized emission that are often apparent as margins of unexpected high or low FRET values around an object (Fig. 7.5B).

Two main sources for this type of deviation exist: chromatic aberrations within the objective and other optics, and, for confocals, slight differences in the collimation of the laser beams. Chromatic aberrations are due to the wavelength dependency of the refractive index of optical glasses, which causes axial misregistration of images taken at different wavelengths [19]. Depending on the objective used, chromatic aberrations may be several micrometers (worst case). Chromatically corrected objectives are available, but it should be stressed that these are optimized only for a limited part of the spectrum, typically the mid-visible range. Therefore, significant chromatic aberration may still be present outside this range. For example, using a good, standard corrected 63×, 1.32 NA oil immersion objective (HCX PL APO CS, #506180, Leica), we noticed focusing deviations of about 400 nm (Fig. 7.5B) between the 430 and 514 nm laser lines used to excite the CFP/YFP FRET pair. Use of a UV-corrected 63× objective (HCX PL APO lbd.BL, #506192, Leica) significantly, but not completely, remedied this chromatic aberration. Chromatic focusing deviations are not limited to violet wavelengths because significant deviations exist for dye pairs excited throughout the visible

spectrum (Table 7.1 in [3]). In addition, chromatic aberrations vary with lens types, and even for different objectives of the same type (L. Oomen and K.J., unpublished; [18]). Axial focusing errors also exist in CCD images but here they usually go unnoticed because of the poor axial resolution of wide-field fluorescence microscopes.

A more generic approach to overcome focusing deviations can be implemented if the setup is equipped for fast fine-focusing. First, **D** and **S** images are recorded at donor excitation. Then, before taking the **A** image at acceptor excitation, the preparation is refocused to minimize chromatic aberration. Because for a given combination of objective and excitation lines the focus deviation is constant, the correction distance needs to be determined only once. We used XZ-scanning of fixed cells or fluorescent beads for this goal. Applying this focus correction in an automated acquisition routine (macro), **D**, **S,** and **A** images are collected from the same focal plane in the biological sample (Fig. 7.5B).

7.4.4. Shading

Lateral intensity errors may be present over the entire image and occur on CCD and confocal systems alike. For CCD systems, a standard correction algorithm exists: corrections are carried out by normalizing pixel intensities using a reference image, a procedure called shading correction [13]. On the confocal system with independent excitation lines, these deviations are often more pronounced because spatial excitation intensities vary independently (L. Oomen, L. Brocks and K.J., unpublished; [18]). For example, when measuring excitation inhomogeneities for the 430 and 514 nm CFP/YFP lines by imaging a solution of the FRET calcium sensor Yellow Cameleon [7], we observed very significant deviations from unity flatness (Fig. 7.6). The 430 nm excitation intensity dropped by as much as 50% at the image corners, while 514 nm deviated by about 15% (data not shown). Importantly, significant differences (up to 20%) also occurred in the center of the images. Deviations of

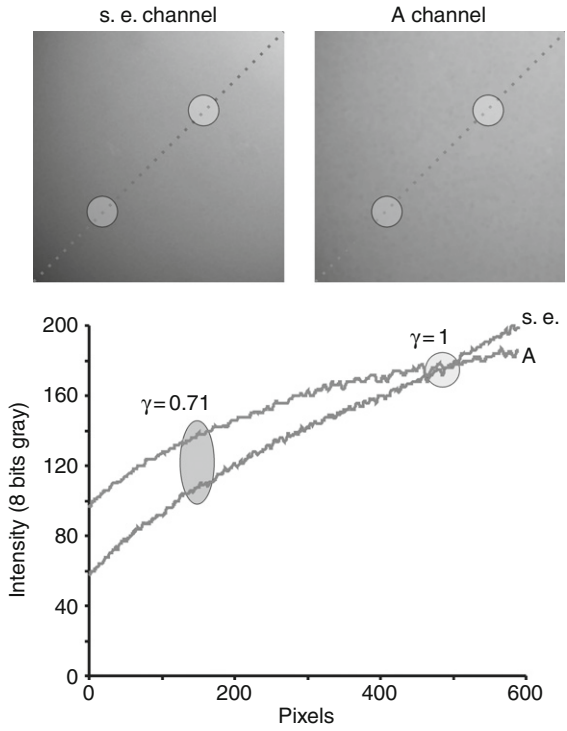

Fig. 7.6. *Shading errors: Lateral image intensity errors*. Shown are parts of reference images (1024 × 1024) that were acquired by averaging eight confocal images of a solution of Yellow Cameleon at 430-nm excitation (upper left panel) and at 514-nm excitation (upper right panel), both detected at 525–570 nm. Note that due to significant differences in shading at these two excitation wavelengths, the γ value (calculated according to Eq. (7.6)) may vary by ~25% in either direction, causing significant errors in calculated FRET. Images were collected with a 63× oil immersion objective without zooming. Note that similar, albeit smaller, differences were observed when 458 and 514 nm laser lines (both derived from the same argon ion laser) were compared.

this magnitude are not uncommon in confocal systems [18], and they are often diminished by increasing the zoom factor.

Shading correction is simply carried out by measuring the fluorescence of solutions of dyes that are spectrally similar to the donor and acceptor. The fluorescence of these reference images is then

normalized to a standard, and all **D**, **S,** and **A** images are divided by their cognate reference standard. Correction factors and FRET images are only calculated after applying the shading correction. In our experience, shading correction is crucial to obtain good FRET images.

7.5. Postacquisition improvements and analysis

When optimal input pictures are obtained whilst observing all the above corrections and precautions, the raw calculated FRET images nonetheless often are quite disappointing and complicated to interpret. See for example the I_S^s, E_D, and E_A images in Fig. 7.3. To blame are noise in the FRET images and the way our eyes handle that.

7.5.1. Noise in FRET images

Even in the nominal absence of laser fluctuations or other image-degrading aberrations, the number of photons that hit the detector during the data collection period of the image (i.e., the exposure time for a CCD image or the pixel dwell time for a confocal image) will contain considerable noise. The photon count x follows a Poisson distribution (Fig. 7.7A) with mean value μ as

$$p(x) = \frac{\mu^x e^{-\mu}}{x!} \tag{7.26}$$

It can be shown that the standard deviation (SD) of this distribution is also just $\sqrt{\mu}$. In other words, if one would repeatedly measure the same pixel that on average collects 100 photons during a single dwell time (a normal value for a rather bright confocal image!!) one would record less than $100–2\times\sqrt{100} = 80$ photons or more than $100 + 2\times\sqrt{100} = 120$ photons just by coincidence in ~5% of the measurements. This uncertainty is expressed as the

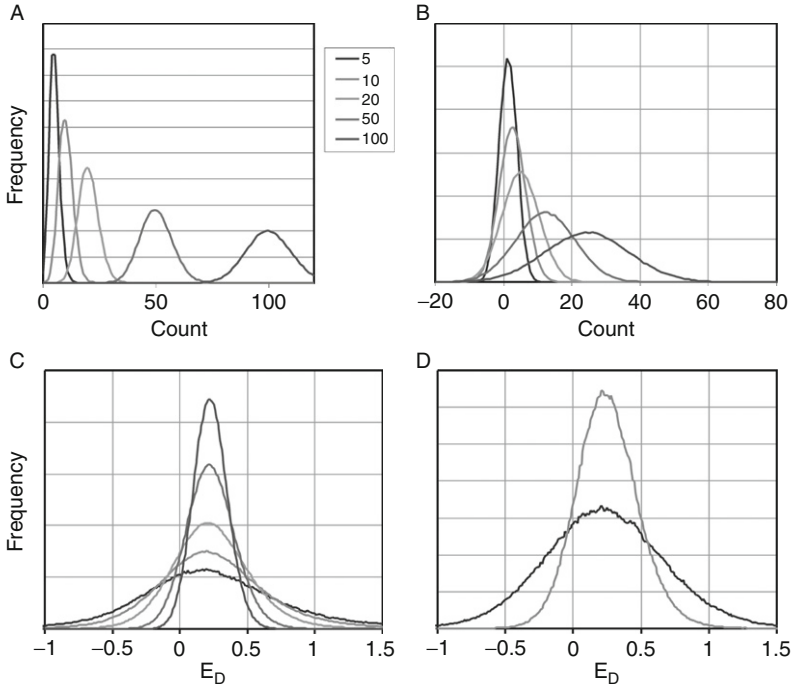

Fig. 7.7. *Effects of Poisson photon noise on calculated SE and FRET values*. (A) Statistical distribution of number of incoming photons for the mean fluorescence intensities of 5, 10, 20, 50, and 100 photons/pixel, respectively. For $n = 100$ (rightmost curve), the SD is 10; thus the relative coefficient of variation (RCV; this is SD/mean) is 10 %. In this case, 95% of observations are between 80 and 120. For example, $n = 10$ the RCV has increased to 33%. (B) To visualize the spread in s.e. caused by the Poisson distribution of pixel intensities that averaged 100 photons for each **A**, **D**, and **S** (right-most curve), s.e. was calculated repeatedly using a Monte Carlo simulation approach. Realistic correction factors were used ($\alpha = 0.0023, \beta = 0.59, \gamma = 0.15, \delta = 0.0015$) that determine 25% FRET efficiency. Note that spread in s.e. based on a population of pixels with RCV = 10 % amounts to RCV = ~60 % for these particular settings! Other curves: for photon counts decreasing as in (A), the uncertainty further grows and an increasing fraction of calculated s.e. values are actually below zero. (C) Spread in E_D values for photon counts as in (A). Note that whereas the value of the mean remains the same, the spread (RCV) increases to several hundred percent. (D) Spread depends not only on photon counts but also on values of the correction

relative coefficient of variation (RCV, defined as the SD divided by the mean value). In this example, RCV = 10%. The situation becomes considerably worse for dimmer pixels (Fig. 7.7A). Thus, in dim sections of the image the degrading influence of noise is worst (Fig. 7.3; see also Fig. 7.8).

As the s.e. values are calculated from individual images, each subject to noise, the errors multiply. This leads to a dramatic spreading of calculated values (Figs. 7.7B and 7.8). Thus, calculated E_D pixel values less than 0 or larger than 1 may be quite common, depending on the intensities of individual images in that pixel and the values of the correction factors. Clearly, such outliers cannot be simply rejected as this would introduce systematic errors in the calculated FRET results. For E_D, s.e. is divided by I_D^d which further increases the spread (Fig. 7.7C). In such pictures, single-pixel RCVs in the order of 100% are not uncommon. It is obvious that the RCV strongly depends on the values of the correction factors α, β, γ, and δ (Fig. 7.7D) and on the magnitude of the FRET efficiency.

Clearly, a major route towards better pictures is to maximize the photon count. On confocal microscopes this can be accomplished in different ways. More photons are collected when increased laser power is used (which incidentally also allows using lower PMT voltages which reduces detector noise). Furthermore, the pinhole can be opened, the dwell time can be increased by lowering the scan speed and acquired images can be averaged. However, these measures come at the expense of increased fluorophore bleaching, prolonged imaging time, and degraded resolution. As this is usually not desired, we will next cover alternative procedures to clear up the images in an—as much as possible—unbiased manner.

In performing the operations described in the next sections, it is absolutely necessary to use imaging software that can handle

factors. For the green trace, mean photon counts for **A**, **D**, and **S** were 30 each. The factors were $\beta = 0.645$ and $\gamma = 0.11$. For the lower trace, counts for **A**, **D**, and **S** were 100, 100, and 30, and correction factor values were $\beta = 0.81$ and $\gamma = 0.4$. Despite higher photon counts, the spread in this example is significantly larger.

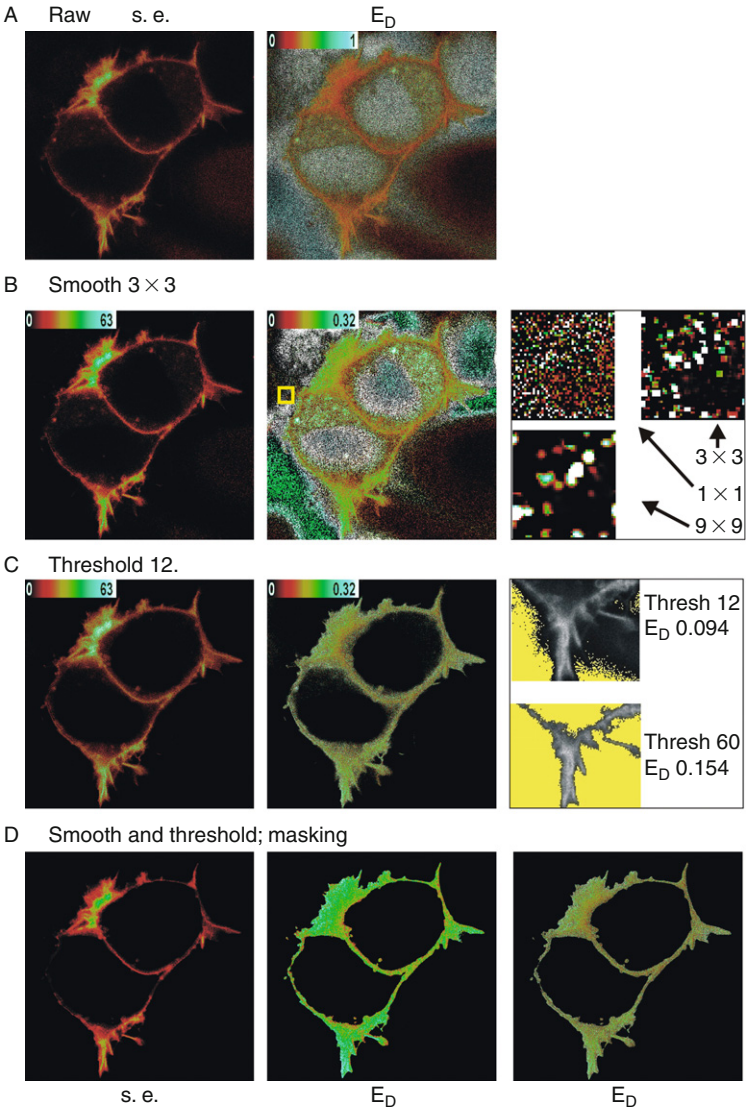

Fig. 7.8. *Postacquisition improvements*. (A) Unaltered "raw" 1024 × 1024 confocal s.e. and E_D images. Note the appearance of excessive noise in E_D at low-signal locations. (B) Lateral averaging (smoothing) using a 3 × 3 kernel

floating point (Negative and broken numbers) calculations. The freeware package Image J (Rasband, W., NIH, Bethesda, Md; *http://rsb.info.nih.gov/ij*) for example performs the described image analysis steps excellently, if 8- or 12-bit images are converted to 32-bit images, and it allows automation of frequently occurring analysis sequences.

7.5.2. Smoothing/filtering

Lateral averaging of the pixel values of the raw images ("smoothing") is the easiest way to reduce the noise effects due to photon statistics significantly, but of course it also reduces the resolution of the picture. A simple mathematical averaging with a 3×3 kernel applied to the background-subtracted, shading-corrected input images already reduces photon noise by ~3-fold (Fig. 7.8A and B). On the other hand, smoothing also spreads out the effect of incidental very high noise pixels that are present in just one of the images (Fig. 7.8B, right detail panels). The effect of this is that it replaces a single outlier pixel in the FRET image with an island of (albeit less pronounced) outliers. To our eye, the effect is the same. Smoothing works better on s.e. images than on the FRET efficiency image. As an alternative, smoothing may be applied to the calculated images as well. It depends on the raw input images which approach gives the best results.

---

cleans up the s.e. image but is less effective on the E_D image. Note the difference in Look-Up Table. Right panel: detail of the middle panel (yellow box) showing how smoothing with the indicated kernel sizes influences E_D. (C) Application of lower threshold on the input images rejects any pixels for which either donor or acceptor intensity is below 12 gray levels. Right panel: the detail taken from the lower portion of the middle panel demonstrates that thresholding significantly influences calculated E_D values. Yellow pixels are excluded from the calculations. (D) A combination of smoothing and thresholding with settings as in B and C cleans up the s.e. and E_D images. Right panel, a mask, derived from the smoothed and thresholded E_D image, is applied to the unfiltered E_D data to preserve fine details in the FRET image.

7.5.3. Thresholding

As the effects of photon noise are most confusing in very dim regions in the image, significant improvements may be expected from simply setting a low-end threshold for each of the input images (Fig. 7.8C). Commonly, separate thresholds have to be set for each of the images, depending on background level and brightness of the image. Indeed thresholding clears up a lot of the noise in background areas, but the highest outliers will still exceed the threshold, and conversely any accidental low-value pixels in the regions that are of interest will be removed. In addition, if the FRET efficiency depends on the expression level of the donor and acceptor constructs [15] thresholding is guaranteed to bias the results. Independent estimation of the magnitude of this bias is necessary. This can be simply performed by comparing calculated FRET values from images differing only in threshold setting (Fig. 7.8C, right detail panels).

Setting an upper threshold may also be necessary. This is evident when saturated pixels are present in the image, a situation that can not always be avoided because expression of some GFP-tagged constructs sometimes causes appearance of extremely bright aggregates in the cytosol that outshine the structures of interest. To retain full dynamic range in the ROI, it is best to allow image saturation in the aggregates while rejecting them from the analysis using an upper threshold. Note that the upper threshold has to be set well below the highest gray level to prevent systematic bias, in particular when the input images are acquired with averaging.

7.5.4. Masking

A masking strategy may be used to dismiss false high FRET values in dim and therefore noisy image regions while simultaneously preventing loss of resolution in the brighter regions (Fig. 7.8D, right panel). In the apparent FRET image, resonance can be distinguished from incidental noise pixels by smoothing the image with a

spatial filter. Isolated noise pixels become averaged out, while consecutive adjacent pixels with positive FRET remain visible. Setting thresholds for each image to just above background intensity generates a mask that contains only regions of true FRET. The thus obtained binary mask may be further edited by for example, erosion, dilation, or floodfill if necessary. The mask is subsequently applied to the original, unfiltered FRET image resulting in near-complete rejection of noise pixels (Fig. 7.8D). Masking tends to be a very powerful way to clean up the images, but since it involves thresholding one has to verify that it does not bias the results in experiments where dimmer pixels are likely to contain less FRET.

7.5.5. Unbiased cleaning up: Mixing FRET efficiency with image intensity information

Completely unbiased visualization of FRET results with strong rejection of noise in dim regions is possible by combining the FRET efficiency picture with the original image intensity (Fig. 7.9A). Here, a pseudocolor RGB FRET image is made from the unprocessed (i.e., without any thresholding or masking) FRET image by overlaying it with a pseudocolor table, also called Look-Up Table or LUT. The intensity of the RGB image is then modulated with the intensity information present in the original input images (see Fig. 7.9). Intensity information may be derived from **D**, **A**, I_S^s or a combination thereof (e.g., the maximum value of **D** or **A**). Thus, background noise pixels that yield high FRET values are still retained in the image, but they will be displayed very dim, just as they appear to the eye.[7] Prior to the modulation step the intensity

[7]Many image analysis packages are not capable to perform this operation correctly in a single step. One approach is to unravel the pseudocolor FRET image into individual R, G, and B channel images. Each of these images is then multiplied with the normalized intensity image, and the final image is regenerated by combining the channels to an RGB image.

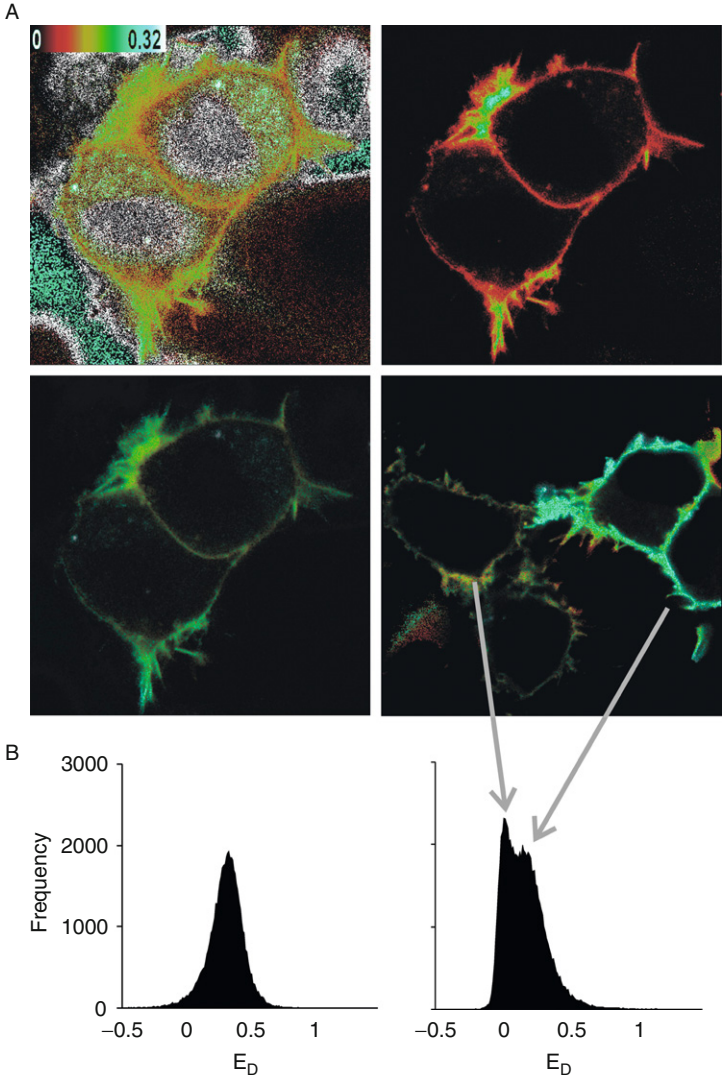

Fig. 7.9. *Further FRET efficiency analysis.* (A) Unbiased display of FRET efficiency. The E_D image (upper left panel) is modulated with an intensity picture (in this case, s.e., upper right panel) to yield the lower left image. See text for further details. Lower right panel, example with several cells

image may optionally be enhanced by smoothing, brightness/contrast adjustment, and masking.

7.5.6. FRET efficiency histograms

A final postanalysis step that helps interpreting the data is to present frequency histograms of pixel FRET values in selected ROI (Fig. 7.8B). As outlined before, correctly acquired and calculated FRET results are expected to display a Gaussian distribution, in first approximation. Inspection of the distribution of FRET values is a quick way to identify possible deviations from this rule. For example, failing to apply proper shading correction may lead to significant broadening of the distribution. In addition, multimodal or very skewed distributions may draw attention to specific problems with the input images or, alternatively, to interesting cell-to-cell variability.

7.6. Discussion

In this chapter, it was shown that filterFRET is an easy, intuitive and quantitative alternative to record sensitized emission and FRET efficiency. The major advantages of filterFRET over donor-based FRET detection methods (FLIM) are that it can be carried out with standard wide-field or confocal fluorescence microscopes that are available in most laboratories, and that it yields additional data on the acceptor population. FilterFRET is also fast, requiring just two confocal scans (if need be on a line-by-line basis) which minimizes the risk of artifacts due to, for example, organelle movement in living cells, and acquisition can be optimized for each channel independently. However, quantitative

displaying different E_D. (B) Frequency histograms of E_D in the pictures in the lower panels in A. Note that whereas the distribution on the left hand displays merely stochastic noise (compare Fig. 7.7C), the rightmost histogram reveals the heterogeneous FRET efficiency in the cells of the corresponding image.

filterFRET requires significant attention for corrections and calibration, whereas FLIM-based FRET techniques are inherently quantitative from first physical principles.

The corrections and calibration of filterFRET differ significantly for CCD microscopes and confocal microscopes. This is because in confocal experiments, channel sensitivities are adjusted at will by the experimenter, and because relative excitation intensities show intended–as well as unintended variations (adjustments and drift, respectively). Confocal filterFRET therefore requires frequent, if not in-line, recalibration; however, if properly streamlined this should not take more than 15 min a day. It also slightly complicates the mathematical framework, as compared to CCD imaging filterFRET. We aimed to arrive at a comprehensive theory that is equally applicable to both imaging modes. We also proposed mathematical jargon that is a compromise between the widely differing terminologies used in the various publications on this topic.

What degree of precision is to be expected from filterFRET? Obviously, precision is governed by the quality of the input pictures, in particular by the lateral and axial co-registration, shading correction, and by photon Poisson noise. For typical confocal images, averaging around a 100 pictures is necessary to arrive at 1% uncertainty in each pixel value of the input pictures, and the FRET calculation will further degrade that figure. Clearly, excessive averaging is not realistic for live-cell imaging. In addition, FPs perform poorly by displaying ill-characterized behavior such as bleaching, maturation, excitation-induced dark states, and pH dependence. Thus, going for one percent variance in pixel FRET values almost certainly stretches the data. However, when multiple pixels can be pooled (average of a ROI), this type of precision may be obtained even without image averaging. Of course, these considerations also hold true for FLIM. From a noise-point of view, simple 2-channel ratio determinations (Sect. 7.22) are preferred. We also want to emphasize again that quantitative FRET efficiency images are not necessarily the ''holy grail'' for cell biologists. For example, if in the soma of the neuron in Fig. 7.1, a kinase-FRET construct would be 100 times more abundant but only half as active

as in the axon, E_D images would suggest half the kinase activity in the soma, whereas sensitized emission images would correctly report a 50-fold enhanced kinase activity.

The area of filterFRET is evolving actively. Recent developments include its combination with other imaging modes including total internal reflection microscopy (TIRF, see also Chap. 9) and FRAP [20]. Furthermore, several laboratories are testing novel FP donor/acceptor combinations to minimize spectral overlap and issues related to FP maturation. In our hands, especially poor red FP (mRFP1, mCherry, and Tomato) maturation interferes with reliable FRET imaging because of the green emission of the immature proteins [17]. In addition, reliable photo-switchable acceptors [21] are an obvious idea with potential. Likewise, correction algorithms keep evolving. For example, Zal and Gasgoigne [6] included correction for photo bleaching in their treatment, and Elangovan et al. [22] introduced concentration-dependency in the leak-through factors. The applicability of such corrections depends very much on imaging conditions and equipment, and we therefore choose not to incorporate them in this chapter. With all these developments, filterFRET has emerged as a full-grown, adaptable, efficient, and fun way to study molecular interactions in vivo.

7.A. Appendix

7.A.1. Factorization

In this appendix, we will assume that a cell expressing donor- and acceptor molecules is excited at appropriate wavelength λ_{ex}^{d} and λ_{ex}^{a} to image FRET. As detailed in the main text, three images are collected that allow independent estimates of cross talk magnitude to perform correction of leak-through:

- **D**, excitation and emission at donor wavelength
- **S**, excitation at donor wavelength and emission at acceptor wavelength
- **A**, excitation and emission at acceptor wavelength

Furthermore, we assume the more general, but also more complex case in which confocal detection is used. This allows for example flexibility in setting independent detector gains for **D**, **S,** and **A**. When this flexibility is not required the expressions simplify considerably.

Before proceeding, an important note must be made. In literature, two different but fully equivalent approaches have been taken in s.e. The first approach considers a cell that contains (unknown) numbers of donors and acceptors N_D and N_A. When energy transfer takes place (be it from collisional encounters or because a stable population of FRET pairs exist with FRET efficiency E) this diminishes the *effective* number of emitting donors with N_S [3]; that is, the FRET efficiency for this population is unity. Thus, the residual donor emission results from $(N_D - N_S)$ unquenched donor molecules, and the N_S population emits *only* sensitized emission. This approach is intuitive in case no assumptions are being made on the presence of a stable population of FRET pairs or on the magnitude of E in a donor–acceptor complex.

A second approach also considers three populations: free (unquenched) donors N_D, free acceptors N_A, and a population engaged in FRET pairs N_S that transfer energy with characteristic efficiency E (between 0 and 1). However, in this case, the N_S population emits *both* donor fluorescence (quenched by a fraction $(1 - E)$) *and* sensitized emission (proportional to EN_S). To keep in line with the treatment and terminology in other chapters in this volume, this latter approach will be followed here. Note, however, that in other chapters the population of FRET pairs is indicated by the subscript $_{DA}$ whereas we stick to the notation N_S to indicate that this quantity is based on photons emitted from sensitized emission (**S** image) and to keep the close synonymy with the former approach. Thus, our I_{D-S} equals I_{DA} and $I_S + I_A$ equals I_{AD}. Both ways yield essentially identical results.

Bearing this in mind, the acquired images are composite images that consist of multiple terms (see Fig. 7.1; for symbols, see Appendix Table 7.A1) as follows:

TABLE 7.A1
Factorization of symbols

Symbol	Factorization
I_D^{d}	$N_D \ell^{\mathrm{d}} \varepsilon_D^{\mathrm{d}} Q_D F_D^{\mathrm{d}} g^{\mathrm{d}}$
I_A^{d}	$N_A \ell^{\mathrm{d}} \varepsilon_A^{\mathrm{d}} Q_A F_A^{\mathrm{d}} g^{\mathrm{d}}$
I_S^{d}	$N_{\mathrm{S}} E \ell^{\mathrm{d}} \varepsilon_D^{\mathrm{d}} Q_A F_A^{\mathrm{d}} g^{\mathrm{d}}$
I_{D-S}^{d}	$(N_D - N_{\mathrm{S}}) \ell^{\mathrm{d}} \varepsilon_D^{\mathrm{d}} Q_D F_D^{\mathrm{d}} g^{\mathrm{d}} + N_{\mathrm{S}}(1-E) \ell^{\mathrm{d}} \varepsilon_D^{\mathrm{d}} Q_D F_D^{\mathrm{d}} g^{\mathrm{d}}$
I_{D-S}^{s}	$(N_D - N_{\mathrm{S}}) \ell^{\mathrm{s}} \varepsilon_D^{\mathrm{d}} Q_D F_D^{\mathrm{s}} g^{\mathrm{s}} + N_{\mathrm{S}}(1-E) \ell^{\mathrm{s}} \varepsilon_D^{\mathrm{d}} Q_D F_D^{\mathrm{s}} g^{\mathrm{s}}$
I_S^{s}	$N_{\mathrm{S}} E \ell^{\mathrm{s}} \varepsilon_D^{\mathrm{d}} Q_A F_A^{\mathrm{s}} g^{\mathrm{s}}$
I_A^{s}	$N_A \ell^{\mathrm{s}} \varepsilon_A^{\mathrm{d}} Q_A F_A^{\mathrm{s}} g^{\mathrm{s}}$
I_A^{a}	$N_A \ell^{\mathrm{a}} \varepsilon_A^{\mathrm{a}} Q_A F_A^{\mathrm{a}} g^{\mathrm{a}}$

The fluorescent components are denoted by I (intensity) followed by a capitalized subscript ($_D$, $_A$, or $_S$, for respectively Donors, Acceptors, or Donor/Acceptor FRET pairs) to indicate the particular population of molecules responsible for emission of I and a lower-case superscript ($^{d,\ a,}$ or ^{s}) that indicates the detection channel (or filter cube). For example, I_D^{d} denotes the intensity of the donors as detected in the donor channel and reads as "Intensity of donors in the donor channel," etc. Similarly, properties of molecules (number of molecules, N; quantum yield, Q) are specified with capitalized subscript and properties of channels (laser intensity, ℓ; gain, g) are specified with lowercase superscript. Factors that depend on both molecular species and on detection channel (excitation efficiency, ε; fraction of the emission spectrum detected in a channel, F) are indexed with both. Note that for all factorized symbols it is assumed that we work in the linear (excitation-fluorescence) regime with negligible donor or acceptor saturation or triplet states. In case such conditions are not met, the FRET estimation will not be correct. See Chap. 12 (FRET calculator) for more details.

– **D** is the output gray scale value after amplification[8] in the donor channel (g^{d}) of the sum of the fraction $\left(F_D^{\mathrm{d}}\right)$ of donor fluorescence in the donor channel and the fraction $\left(F_A^{\mathrm{d}}\right)$ of acceptor fluorescence in the donor channel. The fluorescence of donors depends on the number of donor molecules (N_D) diminished by

[8]The factor g may account for integration time and electron multiplication in CCD imaging, or for the PMT gain in confocal imaging.

those donors that lose their excited state energy due to FRET (EN_S), the molar extinction coefficient of the donor ($\varepsilon_D^{\mathrm{d}}$), the laser intensity ($\ell^{\mathrm{d}}$) at $\lambda_{\mathrm{ex}}^{\mathrm{d}}$, and the donor quantum yield (Q_D). The fluorescence of acceptors depends on their quantum yield (Q_A), and on the sum of the number of acceptor molecules (N_A) cross-excited at $\lambda_{\mathrm{ex}}^{\mathrm{d}}$ ($\ell^{\mathrm{d}}\varepsilon_A^{\mathrm{d}}$) and those excited by FRET ($N_S E$).

$$\begin{aligned}\mathbf{D} = {} & (N_D - \mathrm{EN_S})\ell^{\mathrm{d}}\varepsilon_D^{\mathrm{d}}Q_D F_D^{\mathrm{d}} g^{\mathrm{d}} + N_A \ell^{\mathrm{d}}\varepsilon_A^{\mathrm{d}} Q_A F_A^{\mathrm{d}} g^{\mathrm{d}} \\ & + E N_{\mathrm{S}} \ell^{\mathrm{d}}\varepsilon_D^{\mathrm{d}} Q_A F_A^{\mathrm{d}} g^{\mathrm{d}}\end{aligned} \tag{7.A1}$$

– **S** is the output gray value after the s.e. channel detector scaling (g^{s}) of the sum of the fractions of donor fluorescence in the s.e. channel (F_D^{s}) and of acceptor fluorescence in the s.e. channel (F_A^{s}). The donor fluorescence depends on Q_D, the excitation efficiency at $\lambda_{\mathrm{ex}}^{\mathrm{d}}$ (that is, $\ell^{\mathrm{s}}\varepsilon_D^{\mathrm{d}}$), the number of donors (N_D), and the population of donors that lose their energy by FRET (EN_S). The fluorescence of acceptors depends on Q_A, the amount of acceptor molecules (N_A) excited with $\lambda_{\mathrm{ex}}^{\mathrm{d}}$ ($\ell^{\mathrm{s}}\varepsilon_A^{\mathrm{s}}$) and on the amount of acceptor molecules excited by FRET ($\mathrm{EN_S}$, which is linear to $\ell^{\mathrm{s}}\varepsilon_D^{\mathrm{s}}$).

$$\begin{aligned}\mathbf{S} = {} & (N_D - \mathrm{EN_S})\ell^{\mathrm{s}}\varepsilon_D^{\mathrm{s}}Q_D F_D^{\mathrm{s}} g^{\mathrm{s}} + N_A \ell^{\mathrm{s}}\varepsilon_A^{\mathrm{s}} Q_A F_A^{\mathrm{s}} g^{\mathrm{s}} \\ & + \mathrm{EN_S} \ell^{\mathrm{s}}\varepsilon_D^{\mathrm{s}} Q_A F_A^{\mathrm{s}} g^{\mathrm{s}}\end{aligned} \tag{7.A2}$$

– Finally, **A** is the output gray value after the acceptor channel[9] scaling (g^{a}) of the fraction of acceptor fluorescence in the acceptor channel (F_A^{a}), which depends on the acceptor quantum yield (Q_A) and on the amount of acceptors N_A excited at $\lambda_{\mathrm{ex}}^{\mathrm{a}}$ ($\ell^{\mathrm{a}}\varepsilon_A^{\mathrm{a}}$), of (usually very minor) contributions of donor fluorescence cross-excited at $\lambda_{\mathrm{ex}}^{\mathrm{a}}$ and leaking into the acceptor channel ($(N_D - \mathrm{EN_S})\ell^{\mathrm{a}}\varepsilon_D^{\mathrm{a}}Q_D F_D^{\mathrm{a}} g^{\mathrm{a}}$) and of sensitized emission resulting from cross-excitation at $\lambda_{\mathrm{ex}}^{\mathrm{a}}$ ($\mathrm{EN}_S \ell^{\mathrm{a}}\varepsilon_D^{\mathrm{a}} Q_A F_A^{\mathrm{a}} g^{\mathrm{a}}$). However, as

[9]Note that in confocal imaging, the PMT will generally be the same physical detector as that of the s.e. channel, but operated at a different gain setting.

$\ell^{a}\varepsilon_D^{a}$ is very small, the latter two (leakthrough and FRET) terms in most cases essentially are zero.

$$\begin{aligned}\mathbf{A} = {} & (N_D - \mathrm{EN_S})\ell^{a}\varepsilon_D^{a}Q_D F_D^{a} g^{a} + N_A \ell^{a}\varepsilon_A^{a} Q_A F_A^{a} g^{a} \\ & + \mathrm{EN_S}\ell^{a}\varepsilon_D^{a} Q_A F_A^{a} g^{a}\end{aligned} \tag{7.A3}$$

As mentioned before, we will assume that a cell expressing donor- and acceptor molecules is excited at appropriate wavelength λ_{ex}^{d} and λ_{ex}^{a} in all three channels, so that the donor and acceptor extinction coefficients in **D** and **S** are the same:

$$\varepsilon_D^{s} = \varepsilon_D^{d} \text{ and } \varepsilon_A^{s} = \varepsilon_A^{d} \tag{7.A4}$$

Note that this is always the case for wide-field and confocal determination where **D** and **S** are collected simultaneously using the same excitation filters or lasers. In case three separate filters are used, care should be taken to match the filters so as to fulfill Eq. (7.A4).

By taking (7.A4) in account, (7.A1)–(7.A3) can be simplified as:

$$\begin{aligned}\mathbf{D} &= pN_D + q\mathrm{EN_S} + rN_A \\ \mathbf{S} &= tN_D + u\mathrm{EN_S} + vN_A, \\ \mathbf{A} &= xN_D + y\mathrm{EN_S} + zN_A\end{aligned}$$

$$\begin{aligned} p &= \ell^{d}\varepsilon_D^{d}Q_D F_D^{d} g^{d} & q &= -p + \ell^{d}\varepsilon_D^{d}Q_A F_A^{d} g^{d} & r &= \ell^{d}\varepsilon_A^{d}Q_A F_A^{d} g^{d} \\ t &= \ell^{s}\varepsilon_D^{d}Q_D F_D^{s} g^{s} & u &= -t + \ell^{s}\varepsilon_D^{d}Q_A F_A^{s} g^{s} & v &= \ell^{s}\varepsilon_A^{d}Q_A F_A^{s} g^{s} \\ x &= \ell^{a}\varepsilon_D^{a}Q_D F_D^{a} g^{a} & y &= -x + \ell^{a}\varepsilon_D^{a}Q_A F_A^{a} g^{a} & z &= \ell^{a}\varepsilon_A^{a}Q_A F_A^{a} g^{a}\end{aligned} \tag{7.A1a–7.A3a}$$

Based on the three basic images, **D**, **A**, and **S**, expressions can be derived for the intensity of donors, acceptors, and sensitized emission in their own channel (i.e., the leak-through- and FRET-corrected quantities I_D^{d}, I_A^{a}, and I_S^{s}, respectively). Subsequently, to obtain FRET efficiency, I_S^{s} will be scaled to I_D^{d} analogous to the treatment in the main text.

7.A.2. Sensitized emission

Below, we work out the situation for $x = y = 0$, since in almost all cases, these factors can be neglected. For image sets in which these factors cannot be neglected a corrected image $\mathbf{A}^*$ must first be determined from $\mathbf{A}$ by subtracting xN_D and $y\mathrm{EN_S}$ (7.A.5). In this case, $\mathbf{A}^*$ should be used in all equations below. If $x = y = 0$ then

$$A = zN_A = I_A^{\mathrm{a}} \tag{7.A5}$$

and

$$N_D = \frac{\mathbf{D}}{p} - \frac{\mathrm{EN}_s q}{p} - \frac{\mathbf{A}r}{zp} \tag{7.A6}$$

and Eqs. (7.A5) and (7.A6) are substituted into the equation for $\mathbf{S}$ (Eq. 7.A2a)), yielding,

$$u\mathrm{EN_s} = S - \left(\frac{\mathbf{D}}{p} - \frac{\mathrm{EN}_s q}{p} - \frac{\mathbf{A}r}{zp}\right)t - \mathbf{A}v/z$$

hence:

$$\mathrm{EN_s} = \frac{\mathbf{S} - \mathbf{D}t/p - \mathbf{A}(v/2 - rt/pz)}{u - qt/p}$$

or

$$\mathrm{EN_S} = \frac{S - D\frac{\ell^{\mathrm{s}}F_D^{\mathrm{s}}g^{\mathrm{s}}}{\ell^{\mathrm{d}}F_D^{\mathrm{d}}g^{\mathrm{d}}} - A\left(\frac{\ell^{\mathrm{s}}\varepsilon_A^{\mathrm{d}}F_A^{\mathrm{s}}g^{\mathrm{s}}}{\ell^{\mathrm{a}}\varepsilon_A^{\mathrm{a}}F_A^{\mathrm{a}}g^{\mathrm{a}}} - \frac{\ell^{\mathrm{d}}\varepsilon_A^{\mathrm{d}}F_A^{\mathrm{d}}g^{\mathrm{d}}}{\ell^{\mathrm{a}}\varepsilon_A^{\mathrm{a}}F_A^{\mathrm{a}}g^{\mathrm{a}}}\frac{\ell^{\mathrm{s}}F_D^{\mathrm{s}}g^{\mathrm{s}}}{\ell^{\mathrm{d}}F_D^{\mathrm{d}}g^{\mathrm{d}}}\right)}{\ell^{\mathrm{s}}\varepsilon_D^{\mathrm{d}}Q_A F_A^{\mathrm{s}}g^{\mathrm{s}}\left(1 - \frac{\ell^{\mathrm{s}}F_D^{\mathrm{s}}g^{\mathrm{s}}\ell^{\mathrm{d}}F_A^{\mathrm{d}}g^{\mathrm{d}}}{\ell^{\mathrm{d}}F_D^{\mathrm{d}}g^{\mathrm{d}}\ell^{\mathrm{s}}F_A^{\mathrm{s}}g^{\mathrm{s}}}\right)} \tag{7.A7}$$

Relating back to Eq. (7.8) from the main text, the sensitized emission gray scale image I_S^{s} is composed of the emission from $\mathrm{EN_S}$, which depends on the acceptor quantum yield Q_A, scaled by factors for sensitized emission channel gain (g^{s}), fraction of acceptor fluorescence in the sensitized emission channel F_A^{s}, and donor excitation efficiency $\ell^{\mathrm{s}}\varepsilon_D^{\mathrm{d}}$;

$$I_S^{\mathrm{s}} = \mathrm{EN_S}\ell^{\mathrm{s}}\varepsilon_D^{\mathrm{d}}Q_A F_A^{\mathrm{s}} g^{\mathrm{s}} = \frac{S - D\frac{\ell^{\mathrm{s}}F_D^{\mathrm{s}}g^{\mathrm{s}}}{\ell^{\mathrm{d}}F_D^{d}g^{d}} - A\left(\frac{\ell^{\mathrm{s}}\varepsilon_A^{\mathrm{d}}F_A^{\mathrm{s}}g^{\mathrm{s}}}{\ell^{a}\varepsilon_A^{a}F_A^{a}g^{a}} - \frac{\ell^{\mathrm{d}}\varepsilon_A^{\mathrm{d}}F_A^{\mathrm{d}}g^{\mathrm{d}}}{\ell^{a}\varepsilon_A^{a}F_A^{a}g^{a}}\frac{\ell^{\mathrm{s}}F_D^{\mathrm{s}}g^{\mathrm{s}}}{\ell^{\mathrm{d}}F_D^{\mathrm{d}}g^{\mathrm{d}}}\right)}{\left(1 - \frac{\ell^{\mathrm{s}}F_D^{\mathrm{s}}g^{\mathrm{s}}}{\ell^{\mathrm{d}}F_D^{\mathrm{d}}g^{\mathrm{d}}}\frac{\ell^{\mathrm{d}}F_A^{\mathrm{d}}g^{\mathrm{d}}}{\ell^{\mathrm{s}}F_A^{\mathrm{s}}g^{\mathrm{s}}}\right)} \tag{7.A8}$$

In Eq. (7.A8), the constants α, β, γ, and δ (see main text and Table 7.A2) are identified as detailed in Eqs. (7.A9)–(7.A12). Values for α, γ, and δ can be deduced from imaging of a sample with only acceptor molecules:

$$\frac{{}^{\mathrm{Acc}}D}{{}^{\mathrm{Acc}}A} = \frac{r}{z} = \frac{N_A\ell^{d}\varepsilon_A^{d}Q_A F_A^{d} g^{d}}{N_A\ell^{a}\varepsilon_A^{a}Q_A F_A^{a} g^{a}} = \frac{\ell^{d}\varepsilon_a^{d}F_A^{d}g^{d}}{\ell^{a}\varepsilon_A^{a}F_A^{a}g^{a}} = \alpha \tag{7.A9}$$

$$\frac{{}^{\mathrm{Acc}}D}{{}^{\mathrm{Acc}}S} = \frac{r}{v} = \frac{N_A\ell^{d}\varepsilon_A^{d}Q_A F_A^{d} g^{d}}{N_A\ell^{s}\varepsilon_A^{d}Q_A F_A^{s} g^{s}} = \frac{\ell^{d}F_A^{d}g^{d}}{\ell^{s}F_A^{s}g^{s}} = \delta \tag{7.A10}$$

$$\frac{{}^{\mathrm{Acc}}S}{{}^{\mathrm{Acc}}A} = \frac{N_A\ell^{s}\varepsilon_A^{d}Q_A F_A^{s} g^{s}}{N_A\ell^{a}\varepsilon_A^{a}Q_A F_A^{a} g^{a}} = \frac{\ell^{s}\varepsilon_A^{d}F_A^{s}g^{s}}{\ell^{s}\varepsilon_A^{a}F_A^{a}g^{a}} = \gamma \tag{7.A11}$$

Where again (compare Textbox 2), $\alpha = \gamma\delta$. Similarly, β is calculated from a sample with only donor molecules:

$$\frac{{}^{\mathrm{Acc}}S}{{}^{\mathrm{Acc}}D} = \frac{t}{p} = \frac{N_D\ell^{s}\varepsilon_D^{d}Q_D F_D^{s} g^{s}}{N_D\ell^{d}\varepsilon_D^{d}Q_D F_D^{d} g^{d}} = \frac{\ell^{s}F_D^{s}g^{s}}{\ell^{d}F_D^{d}g^{d}} = \beta \tag{7.A12}$$

Note that when **S** and **D** are collected simultaneously (typically for confocal imaging) β and δ are independent of relative laser line intensities.

Analogous to Eq. (7.8) (text) we can thus rewrite Eq. (7.A8) as:

$$I_S^{\mathrm{s}} = \frac{S - \beta D - \gamma A(1 - \beta\delta)}{1 - \beta\delta} \tag{7.A13}$$

Eqs. (7.A8) and (7.A13) are valid not only in case there is a single FRET population N_{S} with characteristic FRET efficiency E, but also when different FRET populations each with different characteristic FRET efficiency E_i are present $\left(N_{\mathrm{S},i}\right)N_{\mathrm{S},i}$. One can

simply verify this by substituting N_S by $\sum_i N_{S,i}$ and $N_S E$ by $\sum_i N_{S,i} E_i$ in Appendix Table 7.A1 and Eqs. (7.A1)–(7.A7).

7.A.3. The unquenched donor image and E_D

To derive an expression for I_D^d (the unquenched donor image), **D** is corrected for leak-through as well as for signal lost to FRET. For this latter correction, the factor ϕ that relates the lost signal I_S^d in **D**, that is $\left(\mathrm{EN_S}\ell^d\varepsilon_D^d Q_D F_D^d g^d\right)$, to the gain I_S^s in **S**, or ($\mathrm{EN_S}\ell^s\varepsilon_D^d Q_A F_A^s g^s$, Eq. (7.A13)) is:

$$\phi = -\frac{\mathrm{EN_S}\ell^d\varepsilon_D^d Q_D F_D^d g^d}{\mathrm{EN_S}\ell^s\varepsilon_D^d Q_A F_A^s g^s} = \frac{-p}{u+t} = -\frac{\ell^d Q_D F_D^d g^d}{\ell^s Q_A F_A^s g^s} \tag{7.A14}$$

or:

$$\mathrm{EN_S}\ell^d\varepsilon_D^d Q_D F_D^d g^d = -\phi \mathrm{EN_S}\ell^s\varepsilon_D^d Q_A F_A^s g^s \tag{7.A15}$$

In order to solve I_D^d, Eq. (7.A1) is rearranged with information from Eqs. (7.A5), (7.A9), (7.A10), and (7.A14):

$$I_D^d = N_D\ell^d\varepsilon_D^d Q_D F_D^d g^d = \mathbf{D} - (\delta+\phi)\mathrm{EN_S}\ell^s\varepsilon_D^d Q_A F_A^s g^s - \alpha\mathbf{A} \tag{7.A16}$$

Combined with Eqs. (7.A8) and (7.A13) this rearranges Eq. (7.A16), which is identical to Eq. (7.13) in the main text.

$$I_D^d = \mathbf{D} - (\delta+\phi)I_S^s - \alpha\mathbf{A} = \frac{\beta\phi+1}{1-\beta\delta}\mathbf{D} - \frac{\phi+\delta}{1-\beta\delta}\mathbf{S} + \gamma\phi\mathbf{A} \tag{7.A17}$$

Also ζ (Eq. (7.14) in main text) can be redefined after substitution of Eqs. (7.A9)–(7.A12) according to Eq. (7.A18):

$$\zeta = \frac{\beta(\delta+\phi)}{(1-\beta\delta)} = \frac{\frac{\mathrm{tr}}{pv} - \frac{t}{u+t}}{1-\frac{\mathrm{tr}}{pv}} = \frac{\frac{F_D^s}{F_A^s}\left(\frac{F_A^d}{F_D^d} - \frac{Q_D}{Q_A}\right)}{1-\frac{F_D^s}{F_A^s}\frac{F_A^d}{F_D^d}} \tag{7.A18}$$

From Eq. (7.A18) it is clear that ζ only depends on filter throughput and the ratio of quantum yields for donor and acceptor and hence is independent on laser or detector gain settings. For a given combination of confocal filter settings and fluorophores ζ is therefore a constant (for our confocal settings, using CFP and YFP, $\zeta = -0.248$). Therefore, using ζ is distinctly advantageous during confocal imaging where excitation intensities and channel sensitivities are varied independently, whereas G (see main text) varies with detector settings. Now, Eq. (7.A17) can be rewritten:

$$I_D^{\mathrm{d}} = N_D \ell^{\mathrm{d}} \varepsilon_D^{\mathrm{d}} Q_D F_D^{\mathrm{d}} g^{\mathrm{d}} = (1+\zeta)\mathbf{D} - \frac{\zeta}{\beta}\mathbf{S} - \gamma\left(\delta - \frac{\zeta}{\beta} + \delta\zeta\right)\mathbf{A} \tag{7.A19}$$

By definition the E_D is calculated from the loss in donor signal, which can be defined from the symbols in Appendix Table 7.A1, and from the experimental images **S**, **D,** and **A** using Eqs. (7.12), (7.15), and (7.A16):

$$E_D = \frac{N_{\mathrm{S}}}{N_D} E \equiv 1 - \frac{I_{D-S}^{\mathrm{d}}}{I_D^{\mathrm{d}}} = \frac{\beta\phi\mathbf{D} - \phi\mathbf{S} + \gamma\phi(1-\beta\delta)\mathbf{A}}{(\beta\phi+1)\mathbf{D} - (\delta+\phi)\mathbf{S} + \gamma\phi(1-\beta\delta)\mathbf{A}}$$

$$= 1 - \frac{\mathbf{D}}{(1+\zeta)D - \frac{\zeta}{\beta}\mathbf{S} - \gamma\left(\delta - \frac{\zeta}{\beta} + \delta\zeta\right)\mathbf{A}} \tag{7.A20}$$

ζ can be reliably determined, for example by acquiring the **D**, **S,** and **A** images before and after complete acceptor photobleaching. Since postbleach **D** is equal to $N_D \ell^{\mathrm{d}} \varepsilon_D^{\mathrm{d}} Q_D F_D^{\mathrm{d}} g^{\mathrm{d}}$ $\left(= I_D^{\mathrm{d}}\right)$ (see Eqs. (7.A1) and (7.A19)), ζ is found from:

$$\zeta = \frac{{}^{postbleach}\mathbf{D} - {}^{postbleach}\mathbf{D} + {}^{postbleach}\mathbf{A}\alpha}{{}^{postbleach}\mathbf{D} - {}^{postbleach}\mathbf{S}\frac{1}{\beta} + {}^{postbleach}\mathbf{A}\left(\frac{\gamma}{\beta} - \alpha\right)} \tag{7.A21}$$

TABLE 7.A2
Definition of correction factors and constants

Factor	Equations	Factorization	Calculate from	Prep	Comments
α	(7.4), (7.A9)	$\frac{\ell^{d}\varepsilon_{A}^{d}F_{A}^{d}g^{d}}{\ell^{a}\varepsilon_{A}^{a}F_{A}^{a}g^{a}}$	$\frac{\mathbf{D}}{\mathbf{A}}$	acc.	Leak-through of cross-excited acc. into **D**
β	(7.5), (7.A12)	$\frac{\ell^{s}F_{D}^{s}g^{s}}{\ell^{d}F_{D}^{d}g^{d}}$	$\frac{\mathbf{S}}{\mathbf{D}}$	donor	Leak-through of donors into **S**
γ	(7.6), (7.A11)	$\frac{\ell^{s}\varepsilon_{A}^{d}F_{A}^{s}g^{s}}{\ell^{a}\varepsilon_{A}^{a}F_{A}^{a}g^{a}}$	$\frac{\mathbf{S}}{\mathbf{A}}$	acc.	Cross excitation of acceptors
δ	(7.7), (7.A10)	$\frac{\ell^{d}F_{A}^{d}g^{d}}{\ell^{s}F_{A}^{s}g^{s}}$	$\frac{\mathbf{D}}{\mathbf{S}}$	acc.	Leak-through of s.e. into **D**
ϕ	(7.12), (7.A14)	$-\frac{\ell^{d}Q_{D}F_{D}^{d}g^{d}}{\ell^{s}Q_{A}F_{A}^{s}g^{s}}$	$-\frac{1+\delta G}{\beta+G}$	sensor[1]	Relates the loss in **D** due to FRET $\left(I_{S}^{d}\right)$ to the gain in **S** due to FRET $\left(I_{S}^{s}\right)$; negative
ρ	(7.A36)	$\frac{\ell^{a}\varepsilon_{D}^{a}g^{a}}{\ell^{s}\varepsilon_{D}^{d}g^{s}}$	$\frac{\mathbf{A}}{\mathbf{S}}$	donor	Relates signal from cross-excited donors in **S** to that in **A** (provided that emission filters are identical)
σ	(7.A26)	$\frac{\varepsilon_{D}^{d}}{\varepsilon_{A}^{d}}$	$-1/\phi\upsilon$	zero-FRET construct	Relates extinction coefficient of donors at λ_{ex}^{d} to that of acceptors at λ_{ex}^{d}
υ	(7.A28), (7.A32)	$\frac{\ell^{s}\varepsilon_{A}^{d}Q_{A}F_{A}^{s}g^{s}}{\ell^{d}\varepsilon_{D}^{d}Q_{D}F_{D}^{d}g^{d}}$	$-1/\phi\sigma$ or $\frac{\beta\mathbf{D}_{0}-\mathbf{S}_{0}}{\delta\mathbf{S}_{0}-\mathbf{D}_{0}}$	zero-FRET construct	Relates the visibility of acceptors in the **S** channel to the visibility of the same number of donors in the **D** channel
ζ	(7.14), (7.22), (7.A18), (7.A21)	$\frac{\frac{F_{D}^{s}}{F_{A}^{s}}\left(\frac{F_{A}^{d}}{F_{D}^{d}}-\frac{Q_{D}}{Q_{A}}\right)}{1-\frac{F_{D}^{s}F_{A}^{d}}{F_{A}^{s}F_{D}^{d}}}$	$\frac{\beta(\delta+\phi)}{(1-\beta\delta)}$ *or:* $-\beta/(\beta+G)$	sensor	Used to relate the loss in **D** due to FRET to the gain in **S** due to FRET; independent from excitation intensity and gain and therefore constant for given filters and fluorophores; negative
G	(7.19), (7.A24)	$\frac{\frac{Q_{D}F_{D}^{s}g^{s}}{Q_{A}F_{A}^{s}g^{s}}-1}{\frac{\ell^{d}F_{A}^{d}g^{d}}{\ell^{s}F_{A}^{s}g^{s}}-\frac{\ell^{d}Q_{D}F_{D}^{d}g^{d}}{\ell^{s}Q_{A}F_{A}^{s}g^{s}}}$	$-\frac{\Delta\mathbf{S}}{\Delta\mathbf{D}}$ or: $-\frac{\beta\phi+1}{\phi+\delta}$	sensor	Alternative constant that relates the loss in **D** due to FRET to the gain in **S** due to FRET used in literature; note that **G** depends on changes in β and δ; positive

[1]Sensor: any single-polypeptide construct (containing the fluorophores to be used in the experiment) that can be induced to change FRET significantly and homogeneously; e.g., Yellow Cameleon in combination with ionomycin.

Alternatively, ζ can be related to G (see main text, Eq. (7.22)):

$$\zeta = -\frac{\beta}{\beta + G} \tag{7.A22}$$

Or conversely, G can be expressed in terms of β, δ, and ϕ by combining Eqs. (7.A22) and (7.A18);

$$\zeta = -\frac{\beta}{\beta + G} = \frac{\beta(\delta + \phi)}{(1 - \beta\delta)} \tag{7.A23}$$

The constant G is isolated:

$$G = -\frac{\beta\phi + 1}{\phi + \delta} = -\frac{\frac{u}{u+t}}{-\frac{p}{u+t} + \frac{r}{v}} = \frac{\frac{Q_D F_D^{\mathrm{s}} g^{\mathrm{s}}}{Q_A F_A^{\mathrm{s}} g^{\mathrm{s}}} - 1}{\frac{\ell^{\mathrm{d}} F_A^{\mathrm{d}} g^{\mathrm{d}}}{\ell^{\mathrm{s}} F_A^{\mathrm{s}} g^{\mathrm{s}}} - \frac{\ell^{\mathrm{d}} Q_D F_D^{\mathrm{d}} g^{\mathrm{d}}}{\ell^{\mathrm{s}} Q_A F_A^{\mathrm{s}} g^{\mathrm{s}}}} \tag{7.A24}$$

from which dependency of G on detector gain is evident.

7.A.4. Direct acceptor excitation and E_A estimation

Apart from the unquenched donor image providing a FRET estimate E_D, another FRET estimate can be deduced directly from the pure sensitized emission $\left(I_S^{\mathrm{s}}\right)$ and direct acceptor excitation $\left(I_A^{\mathrm{a}}\right)$ components. From Appendix Table 7.A1, the following ratio can be defined[10]:

$$E_A \equiv \frac{N_{\mathrm{S}}}{N_A} E = E \frac{N_{\mathrm{S}} \ell^{\mathrm{s}} \varepsilon_D^{\mathrm{d}} Q_A F_A^{\mathrm{s}} g^{\mathrm{s}}}{N_A \ell^{\mathrm{a}} \varepsilon_A^{\mathrm{a}} Q_A F_A^{\mathrm{a}} g^{\mathrm{a}}} \frac{1}{\gamma\sigma} = \frac{I_S^{\mathrm{s}}}{I_A^{\mathrm{a}}} \frac{1}{\gamma\sigma} \left(= \frac{I_S^{\mathrm{s}}}{I_A^{\mathrm{s}}} \frac{1}{\sigma} \right) \tag{7.A25}$$

where

$$\sigma = \frac{\varepsilon_D^{\mathrm{d}}}{\varepsilon_A^{\mathrm{d}}} \tag{7.A26}$$

[10]Note the similarity of equation A25 between brackets and Eq.equation (16) of Chap. 1.

Combining Eqs. (7.A25) with (7.A5) and (7.A13) yields

$$E_A = \frac{I_S^{\mathrm{s}}}{\gamma\sigma A} = \frac{\mathbf{S} - \beta\mathbf{D} - \gamma\mathbf{A}(1-\beta\delta)}{\gamma\sigma(1-\beta\delta)\mathbf{A}} \tag{7.A27}$$

Hence the quantity of E_A can be simply calculated from the corrected sensitized emission image and the acceptor only image provided the ratio of the molar extinction coefficients of the donor and acceptor at the donor excitation wavelength is known (σ). This quantity can be determined from absorption spectra of purified labeled components or can be experimentally determined as follows. First, let us define a factor υ that relates the signal of N acceptors in the **S** channel to the signal of the same number of donors in the **D** channel:

$$\upsilon = \frac{v}{p} = \frac{N\ell^{\mathrm{s}}\varepsilon_A^{\mathrm{d}}Q_A F_A^{\mathrm{s}} g^{\mathrm{s}}}{N\ell^{\mathrm{d}}\varepsilon_D^{\mathrm{d}}Q_D F_D^{\mathrm{d}} g^{\mathrm{d}}} = \frac{1}{-\phi\sigma} \tag{7.A28}$$

One easy way to determine υ is by using a donor–acceptor fusion chimera that displays no detectable FRET. In this case, $N = N_D = N_A$ and $N_{\mathrm{S}} = 0$, and Eqs. (7.A1a) and (7.A2a) simplify to:

$$\mathbf{D}_0 = pN + rN \tag{7.A29}$$

$$\mathbf{S}_0 = tN + vN \tag{7.A30}$$

Combining Eqs. (7.A29) and (7.A30) with (7.A28), (7.A10), and (7.A12) it follows that:

$$\frac{\mathbf{S}_0}{\mathbf{D}_0} = \frac{t+v}{p+r} = \frac{\frac{t}{p}+\frac{v}{p}}{1+\frac{r}{v}\frac{v}{p}} = \frac{\beta+\upsilon}{1+\delta\upsilon} \tag{7.A31}$$

Here υ can be isolated to yield:

$$\upsilon = \frac{\beta\mathbf{D}_0 - \mathbf{S}_0}{\delta\mathbf{S}_0 - \mathbf{D}_0} \tag{7.A32}$$

7.A.5. The corrected acceptor image

For the acceptor image $\left(I_A^{\mathrm{a}}\right)$ it suffices in almost all cases to simply use the **A** image, because the donor excitation at acceptor wavelength is essentially zero. However, in special cases (e.g., when FRETting between spectrally similar FPs such as CFP and GFP) $\varepsilon_D^{\mathrm{a}}$ may be larger and it may become necessary to correct for the leak-through terms. To accommodate such cases, we here derive **A***, a leak-through-corrected version that than must replace **A** in all calculations.[11] First, copy the expressions for **A** and **S** (Eqs. (7.A2a), (7.A3a), using (7.A4)), substituting (see note 3)F_A^{s} by $F_A^{\mathrm{a}'}$ and F_D^{s} by $F_D^{\mathrm{a}'}$:

$$\begin{cases} \mathbf{S} = t' N_D + u' N_{\mathrm{S}} E + v N_{\mathrm{a}} \\ \mathbf{A} = x N_D + y N_{\mathrm{S}} E + z N_{\mathrm{a}} \end{cases} \tag{7.A33}$$

with

$$\begin{aligned} t' &= \ell^{\mathrm{s}} \varepsilon_D^{\mathrm{d}} Q_D F_D^{\mathrm{a}} g^{\mathrm{s}}, \\ u' &= -t' + \ell^{s} \varepsilon_D^{\mathrm{d}} Q_A F_A^{\mathrm{a}} g^{\mathrm{s}}, \\ \rho &= \frac{x}{t'} = \frac{y}{u'} = \frac{\ell^{\mathrm{a}} \varepsilon_D^{\mathrm{a}} g^{\mathrm{a}}}{\ell^{\mathrm{s}} \varepsilon_D^{\mathrm{d}} g^{\mathrm{s}}} \end{aligned} \tag{7.A34}$$

From combining Eqs. (7.A10), (7.A33), and (7.A34) it can be shown that:

$$\mathbf{A}^* = z N_A = \frac{\mathbf{A} - \rho \mathbf{S}}{1 - \rho \gamma} \tag{7.A35}$$

Note that this equals Eq. (7.8a) of [1].

[11] This is straightforward in case the **A** and **S** filters are identical (i.e., $F_A^{\mathrm{a}} = F_A^{\mathrm{s}}$ and $F_D^{\mathrm{a}} = F_D^{\mathrm{s}}$). With confocal FRET this is commonly the case; with CCD imaging, it requires matching the filters. Without this assumption, an analogous result can be obtained, although derivation is significantly more complicated.

ρ can be determined experimentally in cells labeled with only donor molecules since:

$$\rho = \frac{^{\text{Don}}\mathbf{D}}{^{\text{Don}}\mathbf{S}} = \frac{x}{t'} = \frac{N_D \ell^a \varepsilon_D^{\text{a}} F_D^{\text{a}} Q_D g^a}{N_D \ell^s \varepsilon_D^d F_D^{\text{a}} Q_D g^s} = \frac{\ell^a \varepsilon_D^a g^a}{\ell^s \varepsilon_D^d g^s} \tag{7.A36}$$

7.A.6. Imaging FRET in tethered constructs using two channels

In this appendix, FRET in tethered constructs (where thus donor: acceptor stoichiometry is exactly 1) is calculated from just two images. Provided that independent estimates of cross talk magnitude are available, and the excitation power in both images is the same, full correction of leak through is possible from images:

- **D**, excitation and emission at donor wavelength
- **S**, excitation at donor wavelength and emission at acceptor wavelength. Approach and terminology are as detailed above, except that $N_D = N_A = N_{\text{S}} = N$ and $\ell^{\text{d}} = \ell^{\text{s}} = \ell$

Hence Eqs. (7.A1a) and (7.A2a) can be rewritten as:

$$\begin{cases} \mathbf{D} = pN + q\text{NE} + rN \\ \mathbf{S} = tN + u\text{NE} + vN \end{cases} \tag{7.A37}$$

This set of equations can be solved for N and NE yielding:

$$\begin{cases} N = \dfrac{q\mathbf{S} - u\mathbf{D}}{(t+v)q - (p+r)u} \\ \text{NE} = \dfrac{(t+v)\mathbf{D} - (p+r)\mathbf{S}}{(t+v)q - (p+r)u} \end{cases} \tag{7.A38}$$

Hence:

$$E = E_D = E_A = \frac{\text{NE}}{N} = \frac{(t+v)\mathbf{D} - (p+r)\mathbf{S}}{q\mathbf{S} - u\mathbf{D}} = \frac{\left(\frac{t}{p} + \frac{v}{p}\right)\mathbf{D} - \left(1 + \frac{r}{p}\right)\mathbf{S}}{\frac{q}{p}S - \frac{u}{p}\mathbf{D}} \tag{7.A39}$$

From Eqs. (7.A1)–(7.3A), and (7.A26) it follows that:

$$q = -p + \frac{\varepsilon_D^{\mathrm{d}}}{\varepsilon_A^{\mathrm{d}}} r = -p + \sigma r \tag{7.A40}$$

$$u = -t + \frac{\varepsilon_D^{\mathrm{s}}}{\varepsilon_A^{\mathrm{s}}} v = -t + \sigma v \tag{7.A41}$$

By referring to Eqs. (7.A10), (7.A12), (7.A14), and (7.A28) it follows that:

$$\delta = \frac{r}{v}; \beta = \frac{t}{p}; \phi = \frac{-p}{u+t}; \upsilon = \frac{v}{p}; \text{and } \upsilon = \frac{-1}{\sigma\phi} \tag{7.A42}$$

Combining Eqs. (7.A40)–(7.A42) yields:

$$\frac{r}{p} = \frac{r}{v}\frac{v}{p} = \delta\upsilon \tag{7.A43}$$

$$\frac{q}{p} = -1 + \sigma\frac{r}{p} = -1 + \sigma\delta\upsilon \tag{7.A44}$$

$$\frac{u}{p} = -\frac{t}{p} + \sigma\frac{v}{p} = -\beta + \sigma\upsilon \tag{7.A45}$$

Substituting Eqs. (7.A42)–(7.A45) into Eq. (7.A39) yields:

$$E = \frac{(\beta+\upsilon)\mathbf{D} - (1+\delta\upsilon)\mathbf{S}}{(\delta\sigma\upsilon - 1)\mathbf{S} - (\sigma\upsilon - \beta)\mathbf{D}} = \phi\frac{(\beta+\upsilon)\mathbf{D} - (1+\delta\upsilon)\mathbf{S}}{(\delta+\phi)\mathbf{S} - (1+\beta\phi)\mathbf{D}} \tag{7.A46}$$

A calibration procedure (using only **D** and **S** images) to yield β, δ, ϕ, and υ has been described in Eqs. (7.A12), (7.A10), (7.19)–(7.20), and (7.A32), respectively.

Acknowledgments

We are indepted to Drs L.Oomen and L. Brocks for sharing unpublished data; to Drs L.Oomen, G. vd. Krogt and M. Langeslag for critical reading and comments and to Dr G. vd. Krogt, B. Ponsioen and W. Zwart for preparation

of samples. Financially supported by NWO, the Netherlands Cancer Society and by the Josephine Nefkens Stichting.

References

[1] Gordon, G. W., Berry, G., Liang, X. H., Levine, B. and Herman, B. (1998). Quantitative fluorescence resonance energy transfer measurements using fluorescence microscopy. Biophys. J. *74*, 2702–13.

[2] Hoppe, A., Christensen, K. and Swanson, J. A. (2002). Fluorescence resonance energy transfer-based stoichiometry in living cells. Biophys. J. *83*, 3652–64.

[3] van Rheenen, J., Langeslag, M. and Jalink, K. (2004). Correcting confocal acquisition to optimize imaging of fluorescence resonance energy transfer by sensitized emission. Biophys. J. *86*, 2517–29.

[4] Wlodarczyk, J., Woehler, A., Kobe, F., Ponimaskin, E., Zeug, A. and Neher, E. (2008). Analysis of FRET signals in the presence of free donors and acceptors. Biophys. J. *94*, 986–1000.

[5] Xia, Z. and Liu, Y. (2001). Reliable and global measurement of fluorescence resonance energy transfer using fluorescence microscopes. Biophys. J. *81*, 2395–402.

[6] Zal, T. and Gascoigne, N. R. (2004). Photobleaching-corrected FRET efficiency imaging of live cells. Biophys. J. *86*, 3923–39.

[7] Miyawaki, A., Llopis, J., Heim, R., McCaffery, J. M., Adams, J. A., Ikura, M. and Tsien, R. Y. (1997). Fluorescent indicators for Ca^{2+} based on green fluorescent proteins and calmodulin. Nature *388*, 882–7.

[8] Ponsioen, B., Zhao, J., Riedl, J., Zwartkruis, F., van der Krogt, G., Zaccolo, M., Moolenaar, W. H., Bos, J. L. and Jalink, K. (2004). Detecting cAMP-induced Epac activation by fluorescence resonance energy transfer: Epac as a novel cAMP indicator. EMBO Rep. *5*, 1176–80.

[9] van der Wal, J., Habets, R., Varnai, P., Balla, T. and Jalink, K. (2001). Monitoring agonist-induced phospholipase C activation in live cells by fluorescence resonance energy transfer. J. Biol. Chem. *276*, 15337–44.

[10] Nagy, P., Vamosi, G., Bodnar, A., Lockett, S. J. and Szollosi, J. (1998). Intensity-based energy transfer measurements in digital imaging microscopy. Eur. Biophys. J. *27*, 377–89.

[11] Tron, L., Szollosi, J., Damjanovich, S., Helliwell, S. H., Arndt-Jovin, D. J. and Jovin, T. M. (1984). Flow cytometric measurement of fluorescence resonance energy transfer on cell surfaces. Quantitative

evaluation of the transfer efficiency on a cell-by-cell basis. Biophys. J. *45*, 939–46.

[12] Wouters, F. S., Verveer, P. J. and Bastiaens, P. I. (2001). Imaging biochemistry inside cells. Trends Cell Biol. *11*, 203–11.

[13] Tomazevic, D., Likar, B. and Pernus, F. (2002). Comparative evaluation of retrospective shading correction methods. J. Microsc. *208*, 212–23.

[14] Chen, H., , Puhl, H. L.III, Koushik, S. V., Vogel, S. S. and Ikeda, S. R. (2006). Measurement of FRET efficiency and ratio of donor to acceptor concentration in living cells. Biophys. J. *91*, L39–L41.

[15] van Rheenen, J., Achame, E. M., Janssen, H., Calafat, J. and Jalink, K. (2005). PIP2 signaling in lipid domains: A critical re-evaluation. EMBO J. *24*, 1664–73.

[16] Clegg, R. M. (1992). Fluorescence resonance energy transfer and nucleic acids. Methods Enzymol. *211*, 353–88.

[17] van der Krogt, G. N., Ogink, J., Ponsioen, B. and Jalink, K. (2008). A comparison of donor-acceptor pairs for genetically encoded FRET sensors: Application to the Epac cAMP sensor as an example. PLoS ONE. *3*, e1916.

[18] Zucker, R. M. and Price, O. (2001). Evaluation of confocal microscopy system performance. Cytometry *44*, 273–94.

[19] Cogswell, C. J. and Larkin, K. G. (1995). The specimen illumination path and its effect on image quality. In: ''Handbook of Biological Confocal Microscopy''(Pawley, J. B., ed.). Plenum press, New York, pp. 127–37.

[20] van Royen, M. E., Cunha, S. M., Brink, M. C., Mattern, K. A., Nigg, A. L., Dubbink, H. J., Verschure, P. J., Trapman, J. and Houtsmuller, A. B. (2007). Compartmentalization of androgen receptor protein-protein interactions in living cells. J. Cell Biol. *177*, 63–72.

[21] Demarco, I. A., Periasamy, A., Booker, C. F. and Day, R. N. (2006). Monitoring dynamic protein interactions with photoquenching FRET. Nat. Methods *3*, 519–24.

[22] Elangovan, M., Wallrabe, H., Chen, Y., Day, R. N., Barroso, M. and Periasamy, A. (2003). Characterization of one- and two-photon excitation fluorescence resonance energy transfer microscopy. Methods *29*, 58–73.